Author/s:
Prathumrat, P;Nikzad, M;Hajizadeh, E;Arablouei, R;Sbarski, I

Title:
Shape memory elastomers: A review of synthesis, design, advanced manufacturing, and emerging applications

Date:
2022-06-01

Citation:
Prathumrat, P., Nikzad, M., Hajizadeh, E., Arablouei, R. & Sbarski, I. (2022). Shape memory elastomers: A review of synthesis, design, advanced manufacturing, and emerging applications. Polymers for Advanced Technologies, 33 (6), pp.1782-1808. https://doi.org/10.1002/pat.5652.

Persistent Link:
https://hdl.handle.net/11343/308156

Received: 4 January 2022 | Revised: 3 February 2022 | Accepted: 14 February 2022

DOI: 10.1002/pat.5652

REVIEW ARTICLE

polymers for advanced technologies WILEY

Shape memory elastomers: A review of synthesis, design, advanced manufacturing, and emerging applications

Peerawat Prathumrat[1] | Mostafa Nikzad[1] | Elnaz Hajizadeh[2] | Reza Arablouei[3] | Igor Sbarski[1]

[1]Department of Mechanical and Product Design Engineering, School of Engineering, Swinburne University of Technology, Hawthorn, Victoria, Australia

[2]Department of Mechanical Engineering, Faculty of Engineering and Information Technology, University of Melbourne, Parkville, Victoria, Australia

[3]Data61, CSIRO, Pullenvale, Queensland, Australia

Correspondence
Mostafa Nikzad, Department of Mechanical and Product Design Engineering, School of Engineering, Swinburne University of Technology, Hawthorn, VIC 3122, Australia.
Email: mnikzad@swin.edu.au

Abstract

Shape memory elastomers (SMEs) are a class of intelligent materials characterized by their ability to deform and recover shapes under applied force and external stimuli. Heat and ultraviolet radiation are examples of the most common external stimuli. With the emerging prevalence of internet of things devices and the ensuing need for smart materials and structures, SMEs provide significant opportunities to support the development of novel applications in robotics, remotely actuated systems, and packages, including those promised for the space industry. To harness the immense potential in the emerging applications of these materials, one approach is the systematic multi-scale modeling coupled with artificial intelligence-assisted design leading to the development of next-generation intelligent systems. This review covers several aspects of the synthesis/materials chemistry and applications of SMEs with a view towards enabling such an approach. The synthesis procedures emphasizing dynamic covalent bond reactions are reviewed. Then, liquid crystalline elastomers are introduced as a specific elastomeric material class that exhibits excellent shape memory characteristics and distinctive transition temperatures. The utilization of advanced manufacturing methods such as additive manufacturing, three-dimensional printing, and the emerging four-dimensional printing technologies assisted by machine learning are detailed in producing and predicting SMEs. Finally, the current trends in the use of SMEs are summarized in areas of industrial and space engineering and biomedical applications.

KEYWORDS
additive manufacturing, industrial applications, polymer composites, shape memory elastomers, smart polymers

1 | INTRODUCTION

Elastomers are a class of polymeric materials that have been synthesized and developed for several decades,[1] owing to their unique viscoelastic properties such as low Young's moduli and higher mechanical strain compared to other materials.[2,3] The molecular structure of elastomers contains partially crosslinked networks, unlike that of other thermosetting materials, which contain highly crosslinked

networks. This partially crosslinked structure typically allows elastomers to behave as amorphous polymers or thermosets.[4] However, elastomers can also be copolymerized or physically mixed to perform in similar fashion to thermoplastics, which suit some applications as they are easy to use in manufacturing, for example, injection or compression molding.[5,6] Currently, these materials are exploited in a wide range of applications such as seals and hoses in the oil and gas industry,[7,8] automotive, agricultural, and medical applications,[9–11] soft robotics,[12,13] and wearable devices.[14] Moreover, elastomers have become essential smart-functional materials, exhibiting shape memory or self-healing effects due to their intrinsically flexible molecular structure.[15,16]

For shape memory applications, elastomers can be engineered or synthesized to provide their molecular structure with a particular capability. Elastomers with shape memory effects are able to deform and recover their shapes moving between original and temporary states.[17,18] This phenomenon occurs when shape memory elastomers (SMEs) are triggered by applied load and external stimuli. Heat and UV radiation are the most commonly used stimuli.[19] To quantify shape memory properties, two distinctive shape memory parameters, that is, shape fixity (R_f) and shape recovery (R_r), can respectively be calculated using the Equations 1 and 2 bellow:

$$R_f = \frac{\varepsilon_u}{\varepsilon_m} \times 100\%, \quad (1)$$

$$R_r = \frac{\varepsilon_u(N) - \varepsilon_p(N)}{\varepsilon_u(N) - \varepsilon_p(N-1)} \times 100\%, \quad (2)$$

where ε_u is the fixed strain of the sample after stress relaxation, ε_m is the maximum applied strain, ε_p is the remaining strain after the recovery process, and N is the number of cycles.

Dynamic covalent bonds (DCBs) have gained widespread attention due to their excellent reversibility and stimuli responsiveness.[20] DCBs can introduce the dynamic bond mechanism into polymeric chains and allow polymeric networks to rearrange their topology when activated by external stimuli. In this regard, DCBs can reversibly break and reform through exposure to heat, light, and pH change. Moreover, they can integrate crosslinked networks such as thermosets to form adaptive covalent networks for smart-functional and stimuli-responsive purposes, for example, shape memory and self-healing effects.[21] The thermodynamic equilibrium constant (K^θ) can describe the reversibility of DCBs.[22,23] Any value of K^θ between 10^{-7} and 10^7 allows DCBs to reverse in a dynamic covalent mechanism process.[24] Nevertheless, an irreversible state of DCBs is achieved when K^θ is outside the above range. A variety of reversible mechanisms have been synthesized in several dynamic-covalent elastomeric systems to address the complications of traditional polymeric networks in processing and recycling.

Liquid crystalline elastomers (LCEs) make up another class of polymeric materials that are studied for their shape memory behaviors thanks to their excellent viscoelasticity, mechanical deformation, actuation properties, and responsiveness to various types of stimuli.[25,26] LCEs can deform and recover their shape when external stimuli are applied. These materials represent a distinct state of matter called a liquid crystal state or mesophase, where the properties of elastomers lie on both crystalline solid and isotropic states. The LCE molecules naturally possess the orientational order needed to align along a common direction, namely the director **n**. However, the positional order can be varied from one to two dimensions depending on the degree of ordering of the mesogens. This characteristic results in anisotropy of the physical properties allowing LCEs to be used in widespread applications.[27] Furthermore, LCEs can be categorized into two subclasses based on their responsiveness to the stimuli, that is, thermotropic and lyotropic mesophases.[28] Thermotropic liquid crystals undergo phase transitions (mesophase) within a certain temperature range. Lyotropic liquid crystals experience phase transitions as a function of liquid crystal concentration in a solvent and temperature change.[29] These characteristics are currently exploited for shape memory effects in many LCE systems.[30,31]

In the last few decades, many technologies have been developed to design and process shape memory materials. Modern technologies such as three-dimensional (3D) and four-dimensional (4D) printing have been used to overcome some limitations associated with the development and performance of SMEs. Three dimensional/four dimensional printing technologies facilitate the design and fabrication of the structure via a computational model,[32,33] which is printed via one of several related procedures such as fused deposition modeling (FDM) and direct ink writing (DIW). In some works, the printed specimens produced by these techniques exhibit better shape memory and mechanical properties compared with the samples made using casting or molding techniques.[34] Currently, 3D/4D printed SMEs are utilized in many novel engineering designs and emerging applications, such as flexible electronics, soft actuators, and deployable devices.[35,36]

Machine learning (ML) is another contemporary technology that has gained more attention in material design since its first development in 1959.[37] This class of artificial intelligence (AI) technologies has been used for modeling novel materials with the desired property for a variety of purposes, such as superalloys for ultra-supercritical power plants,[38] shape memory alloys (SMAs),[39] and new solid catalytic materials.[40] Lately, ML-assisted molecular design for shape memory polymers (SMPs) and SMEs has become increasingly common. Using ML has advantages in terms of reducing time in trial-and-error experiments or molecular dynamic (MD) simulations, increasing the chances of success without sacrificing material resources, and addressing the lack of current constitutive models of property predictions. In this regard, many researchers employ ML to design novel SMPs with targeted characteristics in conjunction with traditional experiments and computational simulations.

In this review article, an overview of SMEs is given including crucial information about their underlying characteristics. Various types of DCBs are described in terms of their chemistry, syntheses, and shape memory characteristics. The LCE class of polymers is covered in terms of underlying characteristics, unique stimuli–response mechanism, and utilization as SMEs. Details of the techniques, procedures, and significant parameters associated with 3D and 4D printing of

SMEs are provided with an emphasis on the related shape memory characteristics. ML technology is detailed in its current use for predicting the molecular mechanism with a targeted shape memory property. Finally, some examples are discussed for the current potential uses of SMEs in industrial engineering and biomedical applications.

2 | OVERVIEWS OF SMEs

SMEs are a class of stimuli-responsive polymers, which have been intensively developed to function as stimuli-responsive materials. These materials possess an ability to return to their original shape after being deformed to another temporary shape, as illustrated in Figure 1.[41,42] This shape memory process can operate under applied force and exposure to external stimuli. Currently, many types of stimuli are being used to stimulate shape memory behaviors, including temperature,[43] pH,[44] light,[45] infrared,[46] water or solvent,[47,48] and electric and magnetic fields.[49–51]

Molecular architecture or molecular deformation mechanism, is another essential factor in achieving shape memory behavior.[52,53] The molecular architecture of SMEs must consist of net-points (the hard phase or fixed phase) and switching units (the soft phase or reversible phase), which allow the structure to be deformed, maintained, and recovered under applied force and external activation.[54,55] Recently, Chien et al.[56] studied shape memory characteristics of SME-based waterborne biodegradable polyurethane. Poly(ε-caprolactone)-poly(L-lactic acid) (PCL−PLLA oligodiol) was used as a mixed reversible phase. However, isophorone diisocyanate was needed as a fixed phase. The PCL/LLA sample showed the highest R_f and R_r of 74.5% and 87% when stimulated by air, respectively, and R_r of 65.5% and 100% when stimulated by different water temperatures of 25°C and 37°C, respectively. SME-based thermoplastic elastomers have been developed by Salaeh et al.[57] This shape memory material was prepared using poly(vinylidene fluoride)/carboxylated nitrile butadiene rubber (PVDF/XNBR) blends containing ionic crosslinks. The samples demonstrated excellent values of R_f and R_r up to 90% and 99%, respectively. It was because both parts of the PVDF-based hard phase and XNBR-based soft phase were responsive to thermal stimulation at 80°C.

Elastomeric composites have been developed to improve some intrinsic properties of SMEs, including shape memory and thermal and mechanical properties. Li et al.[58] have polymerized SME by using dodecanedioic acid (DDDA)-based hyperbranched prepolymer with lignin. Diacid DDDA worked as a reversible phase. However, lignin was responsible for a fixed phase. Their results demonstrated excellent R_f and R_r, which were above 80% in all considered mass ratios of lignin. The thermal and mechanical properties of this polymeric system increased with an increase in the lignin mass content. Glass transition temperature (T_g) increased from 5.3°C to 16.8°C with a lignin mass content between 0 and 35 wt%. This composite material exhibited the highest tensile strength at 5.3 MPa, Young's modulus at 8.9 MPa, strain at break of 301%, and toughness at 1.03 GPa with 30 wt% lignin contents.

Thakur and Karak[59] have studied R_r and recovery time of a tough elastomeric hyperbranched polyurethane/reduced graphene oxide (HPU/RGO) nanocomposite system. This system was synthesized via an in-situ polymerization technique, which varied the mass content of RGO between 0.5 and 2.5 wt%. Shape memory properties were characterized using three external stimuli, including microwave, light, and heat. The results showed that the samples with 0.5 wt% of RGO responded to microwave with shape recovery in 80 s. However, these samples were recovered by activation of light and heat within 150 and 300 s, respectively. In another work, Du et al.[60] studied the effects of stearic (SA) mass content and the chemo-responsibility of a triple-shape memory polyolefin (POE)/SA elastomeric composite. The POE/SA composites were melt-blended by twin-screwed extruder in temperatures between 100 and 150°C. The mass content of SA was varied from 10 to 50 wt%. The 50/50 wt% POE/SA showed excellent triple-shape memory characteristics with R_f of 82% and 86% for first and second temporary shapes, respectively. At the same time, R_r of this material was 91% and 98% for returning to the first temporary and original shapes, respectively. Moreover, this POE/SA sample exhibited elongation at break of 600% and tensile strength of 7 MPa.

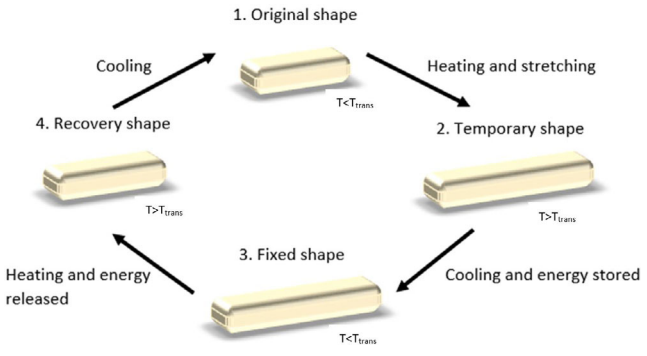

FIGURE 1 Schematic representation of the deformation of a shape memory cycle

3 | SYNTHESES OF SMEs

SMEs can be synthesized by physical or chemical crosslinks to construct net-points and switch units onto the polymeric chains. Dynamic covalent chemistry is a potential synthesis technique that can generate adaptable bonds between these two segments. This dynamic chemistry can reversibly break and reform bonds when emerging either automatically or under response to stimuli such as light, pH, and heat. Typically, dynamic covalent bonds (DCBs) are static at room temperature and can be dynamic by external activation.[61] DCBs are able to re-stabilize their irreversible covalent bonds when activation is removed.[24] This is beneficial for elastomeric chains as smart-functional materials, for example, shape memory and self-healing elastomers. Moreover, elastomers with DCBs have the potential to enhance the sustainability of the 3D printed samples and perform as

the reactive sites for post-printing derivatization.[62] Therefore, DCBs have gained attention in both academic and industrial applications to develop novel SMEs with distinct shape memory effects. Currently, DCBs can be synthesized via several types of chemical reactions, including disulfide metathesis,[63,64] olefin metathesis,[65,66] transcarbamoylation,[67,68] boronic ester chemistry,[69] Diels-Alder reaction,[70,71] and thiol-ene reaction.[72,73] This section focuses on DCB syntheses and their chemistry to produce adaptive mechanisms for elastomers-based shape memory materials.

3.1 | Disulfide metathesis

Disulfide metathesis or disulfide exchange reaction has been widely used to form DCBs to generate the dynamic functionality of elastomeric polymers.[74] In the case of shape memory applications, this reaction can encourage chemical movement of the linkages in the polymer chains. This chemical bond can respond to water and heat allowing the shape recovery of SMEs. However, shape fixity can be maintained under redox or UV irradiation.[75] This reaction contains many advantages such as resistance to environmental degradation, good adhesion, and easy for processing.[76] Generally, this reaction can be classified into two classes, namely, anionic and radical reactions.[61]

3.1.1 | Disulfide anionic reactions

In a disulfide anionic reaction mechanism, thiolate anions can break original disulfide bonds and reform them with other disulfide bonds when the catalysts or base conditions are applied.[63,77] Zhang et al.[78] have investigated the effects of disulfide bonds on a hard phase (netpoints) of polyurethane (PU), which was synthesized via a two-step method. First, methylene diphenyl isocyanate (MDI) and polytetrahydrofuran (pTHF) were mixed to generate urethane functional groups at 60°C under an inert atmosphere. Dibutyltin dilaurate (DBTDL)-based catalyst was added to aid the reactivity. Second, 2,2′-dithiodiethanol or 1,4-butanediol were subsequently used as chain extenders for creating DCBs. The results show that this DCB synthesis technique generated shape memory effects when stimulated over its melting temperature of 150°C allowing these samples to exhibit shape memory characteristics. Moreover, a synthesis method with a single type of chain extender (2,2′-dithiodiethanol or 1,4-butanediol) was shown to have higher thermomechanical properties than mixed chain extenders.[78]

3.1.2 | Disulfide radical reactions

The radical transfer process and crossover reactions can generate the adaptive disulfide bonds associated with light or a radical reactor in this reaction.[79,80] Michal et al.[81] have developed polydisulfide networks, which possess both shape memory and self-healing behaviors. This elastomeric material was synthesized to form a semicrystalline, covalently crosslinked film by employing a photoinitiator to generate bisthiol oligomers in the first stage. Then, the oligomer was dissolved in 40 ml of tetrahydrofuran (THF) and a tetrathiol crosslinker was added by oxidative coupling of the thiol moieties using sodium iodide (NaI)/ hydrogen peroxide (H_2O_2). The samples were cured at room temperature overnight to obtain a gel. Finally, the gel was shaped as a film by compression molding at 180°C for 40 min. The polymeric films revealed shape memory behaviors when stimulated by light or temperature above 180°C. A scheme of the synthesis route and a process of shape memory behaviors is illustrated in Figure 2.

3.2 | Olefin metathesis

Olefin metathesis is an organic reaction that can generate dynamic covalent networks between alkenes (olefin).[82,83] This reaction encourages redistribution of olefin fragments by dividing and reforming carbon–carbon double bonds using catalysts under ambient conditions.[65,84] This metathesis typically requires heterogeneous metal-catalysts to activate the progress of the reaction, that is, organoaluminium or organotin compounds, molybdenum and ruthenium.[85,86] However, in some studies, homogenous metal-catalysts have been used to proceed the reaction, for instance, Schrock or Grubbs catalysts.[87–90] This reaction can also be realized using homogeneous accelerators such as (a) Schrock catalysts featuring molybdenum(VI)- and tungsten(VI) -based centers connected alkoxide and imido ligands and (b) Grubbs catalysts containing ruthenium(II) carbenoid complexes. Olefin metathesis has benefits in terms of cost-effectiveness, high yielding process, being environmentally friendly, and being scalable from milligram to multi-ton.[91]

Recently, Del Rio et al.[92] have investigated shape memory properties of polyurethane where it is synthesized using polyols based glyceryl triundec-10-enoate. Figure 3 illustrates a schematic of the acyclic triene metathesis polymerization (ATMET), a subclass of olefin metathesis. Glycerol and methyl undec-10-enoate were blended to polymerize glyceryl triundec-10-enoate by using a homogeneous Hoveyda-Grubbs second-generation catalyst. A methyl acrylate-based chain stopper was then added to the system to suppress the reaction. Eventually, polyols were reacted with methylene diphenyl diisocyanate (MDI) to synthesize polyurethane samples. In their results, R_f and R_r of this system were in the range of 70% to 95% and 75% to 99%, respectively.[92]

Del Rio et al.[93] have synthesized a similar elastomeric system using acyclic diene metathesis (ADMET) polymerization. Polyols were prepared by a reaction of 1,3-di10-undecenoxy-2-propanol and 10-undecenol. Lithium aluminum hydride ($LiAlH_4$) was employed as a reducing agent. Linear polyols acquired from this process were then polymerized with MDI to yield amorphous and semicrystalline regions in PU networks. This polymeric system also exhibited excellent ratios of shape memory characteristics with a tensile deformation yielding $R_f = 94\%$ and $R_r = 88\%$, excellent thermal stability above 400°C, and good mechanical properties, for example, Young's modulus up to 90 MPa and elongation at break up to 171%.[93]

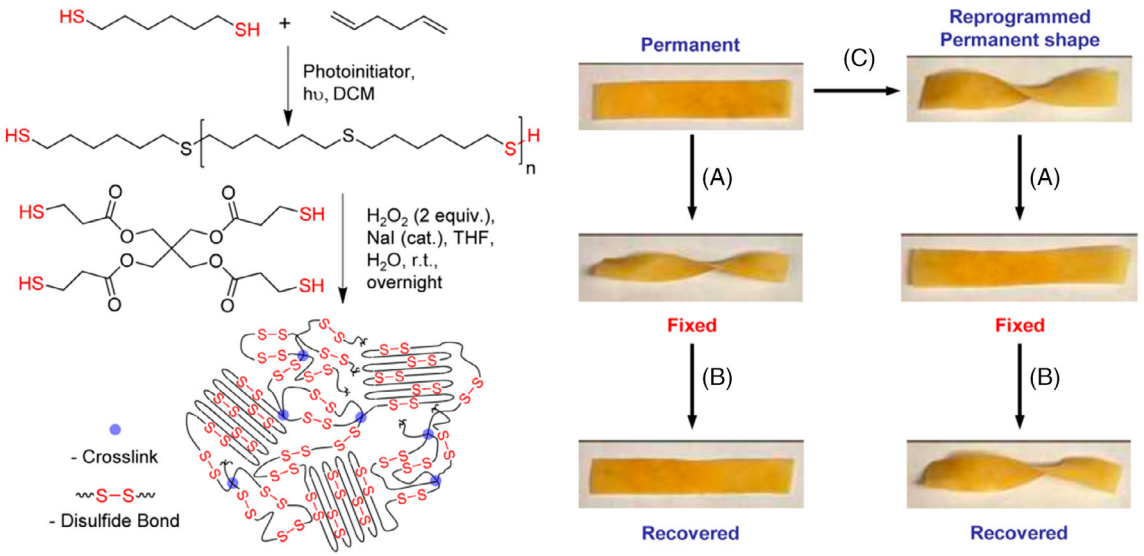

FIGURE 2 Synthesis of the semicrystalline polydisulfide network (left) and shape memory process (right). A permanent sample in a thin film was heated to 80°C to deform a helical shape and fix this temporary shape at low temperature (A), the film was then reheated at 80°C to recover to the permanent shape (B). A permanent sample can also be deformed via photoprogramming by holding it in the helical shape while exposing it to UV light (C). Reproduced with permission from Michal et al.[81]

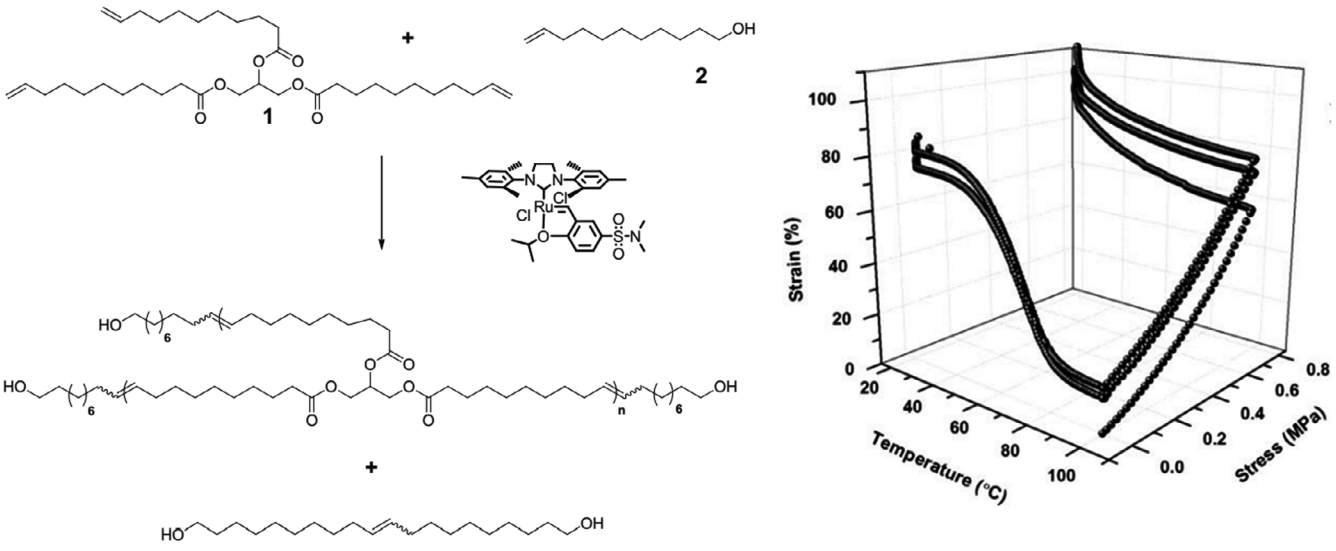

FIGURE 3 Schematics of a synthesis route of branched polyols via acyclic triene metathesis polymerization metathesis of triglyceride **1** with chain stopper **2** (left) and a stress–strain shape memory cycle of polyurethane (right). Reproduced with permission from Del Rio et al.[92]

3.3 | Transcarbamoylation

Transcarbamoylation reaction is a non-enzymatic post-translational modification (PTM) in which cyanate (OCN^-) functional groups react with N-terminal amino groups (NH_3^+).[94,95] Typically, this biochemical reaction involves many biological processes such as enzyme reaction, protein–protein interactions, and protein transport.[94] This reaction is contrast to transesterification, where transesterification is the reaction of exchanging the R″ group of an ester with the R′ group of an alcohol by using a catalyst. Transcarbamoylation can be adopted as a DCB for shape memory applications. Zheng et al.[67] have developed polyurethane (PU) that contains carbamate bonds where they can be active structural moieties in PU networks. This reaction requires three reactants, that is, poly(ethylene glycol) diol (PEG), hexamethylene diisocyanate (HDI), and glycerine (GLY), to polymerize shape memory PU. A dynamic transcarbamylation reaction is shown in Figure 4. The rheological behavior of this dynamic covalent reaction is a vital factor affecting the shape deformation process. The viscosity of this network exhibits a constant value at low strain rates and varies slightly with increasing strain rates, unlike that of other polymer melts. The dynachemorheology behavior is selected to describe the bond breaking and reformation for this reaction. Figure 4 indicates a process of

shape memory measurement where R_f and R_r of the elastomeric system are up to 98% and 99%, respectively.[67]

3.4 | Boronic ester chemistry

A boronic acid is a Lewis acid generated by one of the three hydroxyl groups of boric acid when substituting an aryl or alkyl group.[96,97] This compound consists of a carbon–boron bond that makes it a member of the organoborane class.[98,99] Due to its Lewis acid characteristics, this class of DCBs can form reversible covalent complexes with sugars, amino acids, hydroxamic acids, or Lewis base donors such as hydroxide, fluoride, amine, and carboxylate group.[100–102] A boronic acid can also form with an alcohol functional group to generate a derivative boronic ester and exhibits dynamic covalent mechanism under ambient conditions.[103,104] Therefore, this chemical bond can perform as a reversible reaction adopted to shape memory mechanism.[61,105] Furthermore, due to low toxicity and bio-functionality of this acid, it is suitable for biomedical applications.[106]

Zhang et al.[69] have implemented a synthesis of polyacrylamide (PAAm)/polyvinyl acetate (PVA)–borate hydrogel system to investigate shape memory characteristics by utilizing high-efficiency borate ester bonds. In Figure 5, polyvinyl acetate (PVA) was dissolved in deionized water. Acrylamide (AAm), potassium persulfate (KPS) based initiator, and methylene bis-acrylamide (Bis) based crosslinker were also mixed into the solution and stirred for several minutes before polymerization at 60°C for 6 h. The samples exhibited shape memory effects when immersed in a borax solution. This material showed a high value of R_f that increased up to 95% with increasing the PVA content. Moreover, R_f increased with by increasing the solvent concentration from 0.01 to 0.08 M. It is likely because excessive borax concentration can cause higher crosslink density of temporary boronate ester bond. The shape memory process unexpectedly became faster under wetter conditions.[69]

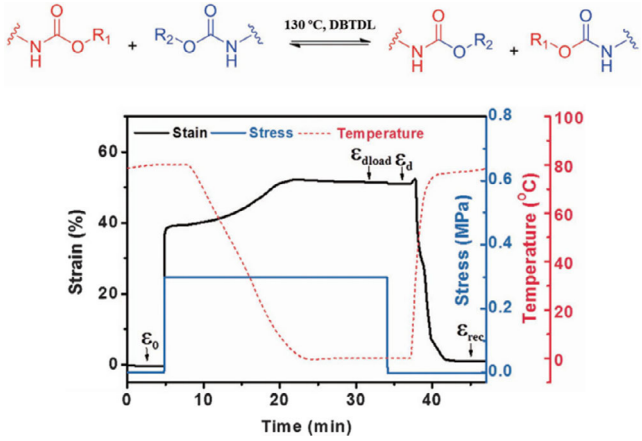

FIGURE 4 A dynamic exchange reaction of transcarbamoylation (top) and a characterization of elastic shape memory process of polyurethane thermosets (bottom). Reproduced with permission from Zheng et al.[67]

3.5 | Diels–Alder reaction

Diels–Alder (DA) reaction is another chemical process that is widely used to generate DCBs in recent years.[107–109] Typically, this reaction consists of a single step of dynamic covalent reaction without the involvement of intermediates. DA reaction has some advantages in terms of increasing reaction rates, stereoselectivity, and regioselectivity. This organic reaction can be generated by a conjugated diene and a substituted alkene, called dienophile, to form a

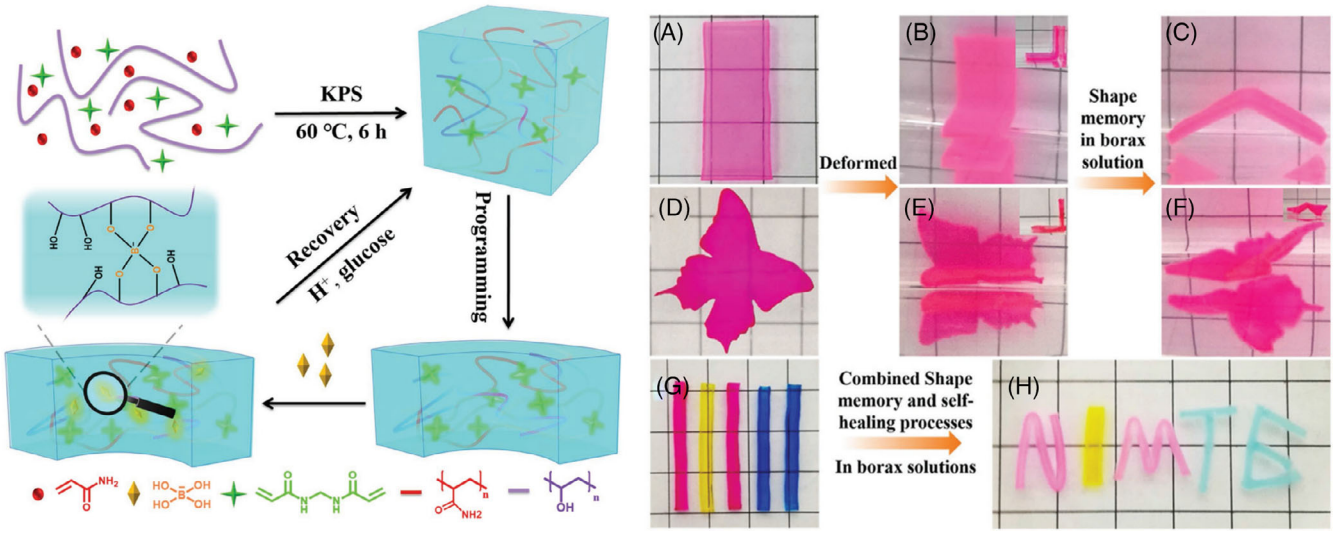

FIGURE 5 A preparation of PPAm/PVA sample and its shape memory mechanism based on the dynamic borax-diol chemistry (left), images of shape memory behaviors of the rectangular and butterfly-shaped specimens (A–F) in borax solution and a combination of dual functions of shape memory and self-healing characteristics in the solution (G,H) (right). Reproduced with permission from Zhang et al.[69]

substituted cyclohexene derivative between 25 and 37°C.[61,110,111] Moreover, it can proceed in the reverse direction at high temperature, that is, a retro-DA (r-DA) reaction. The formation of furans and maleimides is an example that shows the r-DA reaction when the initial reactants are heated up to 110°C.[112,113] In this reaction, temperature plays a critical role in reversibility without any catalyst involvement making this reaction environmentally benign. Therefore, a combination of DA and r-DA reactions, called DA/r-DA adducts, can be used in dynamic covalent polymers with temperature changes.

Zhao et al.[114] have synthesized DA bonds between the crosslink points of poly(siloxane-urethane) elastomers to bring about self-healing and shape memory effects. DA reactions were used to synthesize diols from maleic anhydride and furan in the synthesis procedure and subsequently polymerize with polydimethylsiloxane (PDMS) and PU. Diol groups of PU networks worked as switch units, while polycaprolactone (PCL) in siloxanes was used as net-points. The samples were investigated for shape memory behaviors in a melting temperature (T_m) region from 43 to 60°C.[114] The specimens exhibited notable shape memory behaviors, as shown in Figure 6. Moreover, these elastomeric specimens were used in films to perform a self-healing test. The film surface, which was cracked by a knife, healed at 140 and 80°C when heated for 30 min and 24 h, respectively. A retro-DA debonding reaction proceeded at 140°C followed by re-bonding in polymer chains via a DA reaction at 80°C. This process results in the repairing of the incision.

Ninh et al.[115] studied shape memory properties of a polyester-based biodegradable elastomer, which was synthesized using DA adducts. A glycerol-co-sebacate (PGS) prepolymer was synthesized via a polycondensation reaction between glycerol and sebacic acid. A Furan modification was then introduced to yield a polyester precursors-based hyperbranched multivalent PGS-Furan (PGSF) network. Finally, DA cycloaddition reactions were used to prepare PGSF-1,1′-(methylenedi-4,1-phenylene)bismaleimide (PGSF-DPBM) networks on maltosecoated silicon oxide handling substrates. A forward DA cycloaddition reaction on this network was proceeded to achieve DA cycloaddition at 37°C. In a shape memory process, a helical-shaped specimen was deformed at T_g of 11.5°C and fixed into a temporary planar shape below this temperature by immersing in cold water. This material then recovered to its permanent helical shape once it was heated to above its T_g.[115]

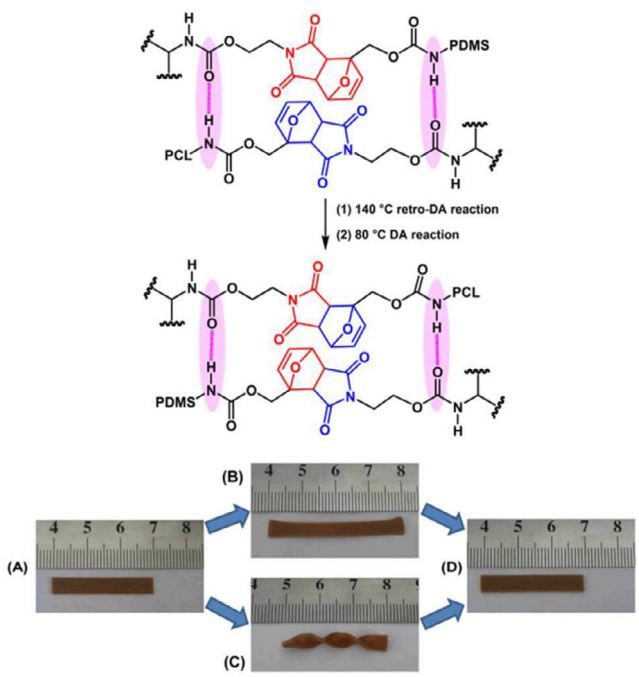

FIGURE 6 A schematic representation of the mechanism of DA/r-DA reaction (top) and a shape memory cycle of polyurethane (PU) via two types of stretch and twist deformation (bottom). Reproduced with permission from Zhao et al.[114]

3.6 | Thiol–ene reaction

Thiol–ene is an organic reaction that has been known for over a century and is widely used for click reactions.[116–118] It is recognized as alkene hydrothiolation, which generates thiolether groups from thiols and alkenes.[119–121] This reaction possesses many advantages including high yield, fast rates, and stereoselectivity.[122] Thiol–ene chemistry can be used as DCBs by two main synthesis techniques. First, the traditional thiol-ene free radical reaction that creates thiyl radical via activation by light, heat, or radical initiators.[123–125] Second, the radical combining with a C═C functional group via an anti-Markovnikov addition creates a carbon-centered radical.[126] Furthermore, this reaction can proceed via a photo-polymerization that is advantageous for many applications including optical components, adhesives, and microdevices.[127,128] However, its main drawback is that its reactivity can be prevented by oxygen inhibition.[129]

Ma et al.[130] have created a novel type of a thiol-ene elastomer via a two-stage photo-polymerization reaction. Pentaerythritol tetrakis(3-mercapto propionate) (PETMP) and tetra(ethylene glycol) diacrylate (TEGDA) were synthesized with triethylamine (TEA) catalyst and photoinitiator (Irgacure 184). Michael-addition polymerization was required to fabricate the thiol-ene specimens in the first step of the reaction. Subsequently, a radical polymerization was proceeded by using 365 nm light with an intensity of 80 W/m^2. The specimens were stretched with 20% strain during this irradiation. The thiol-ene bonds of this system were rearranged as a result and exhibited shape memory characteristics via 405 nm light irradiation.[130]

In a similar reaction, a thiol-Michael reaction can occur between an electron-deficient C═C and a thiol at the presence of a weak base or nucleophile catalyst.[61,131] In this reaction, thiol combines with the base catalyst to generate the deprotonation of the thiol group. This step creates a thiolate nucleophile and ammonium cation. The nucleophile is then reacted with an electrophilic C═C bond to form an intermediate anion. Eventually, this anion attracts a free proton from the first stage to yield the thiol-ene functional group.[132] This thiol-Michael adduct can effectively respond to heat and pH.[133,134]

Lewis et al.[135] have synthesized a series of shape memory materials from an acrylate-terminated PCL system using the thiol-Michael

reaction. In the synthesis method, three-arm PCL prepolymers were synthesized by ring-opening polymerization of caprolactone at 120°C under a continuous N_2 atmosphere for over 24 h. Glycerol and tin(II) octoate ($SnOct_2$) were used as a trifunctional initiator and a catalyst, respectively. Then, hydroxy-terminated prepolymer was reacted with acryloyl chloride via nucleophilic substitution to form a three-arm acrylate prepolymer at 80°C for 48 h. The product was eventually vacuum-dried at 60°C overnight. The samples exhibited excellent shape-memory behaviors, for example, R_f up to 80% and R_r up to 100%, as depicted in Figure 7. Moreover, the specimens indicated remarkable mechanical properties, that is, elongations to failure up to 400%.[135]

3.7 | Transesterification

Transesterification is another class of organic reactions widely used from laboratory to industrial scale due to its economic and low temperature and pressure requirement during the process.[61] The reaction mechanism of transesterification is that an R′ group of an ester is exchanged with an R″ group of alcohol to form a new ester and alcohol by using Lewis acids or strong base catalysts. This dynamic covalent reaction can also be occurred by other methods such as using an enzymatic catalyst and supercritical fluid techniques.[136–138] In industrial scale, this reaction is typically utilized in polyester production, methanolysis and biodiesel production, and fat processing. Furthermore, this reaction has many advantages such as well-controlling, high conversion and rate, and being environmentally friendly.

Recently, transesterification has been exploited to generate DCBs in elastomeric systems for shape memory applications. Feng et al.[139] have fabricated photo-induced shape memory characteristics of epoxy natural rubber (ENR)-based vitrimers. These bio-materials have outstanding advantages such as good mechanical properties, weather resistance, air impermeability, and recyclability. In the synthesis process, ENR was crosslinked by dodecanedioic acids (DA) via transesterification reaction. A small amount of aniline trimer (ACAT) was added to the system for bifunctional purposes, including accelerating transesterification reaction and making the samples respond to pH and light. The R_f and R_r of these vitrimers were above 95% in the reconfiguration process with light activation. In addition, Gao et al.[140] have synthesized semicrystalline poly(ethylene-co-vinyl acetate) (PEVA) with dynamic covalent bonds. Typically, PEVA is widely used as commercial polyolefin products such as table coverings, cosmetic bags, and electric heaters. In this case, this material was used for SMEs due to its broad melting temperature. In the reaction mechanism, the ester linkages in the PEVA structure could act as DCBs when a transesterification catalyst was introduced. The PEVA samples exhibited shape memory behaviors when stimulated by heat between 0 and 50°C under a stress-free condition. The samples can be exploited for 5 cycles via a shape memory process.

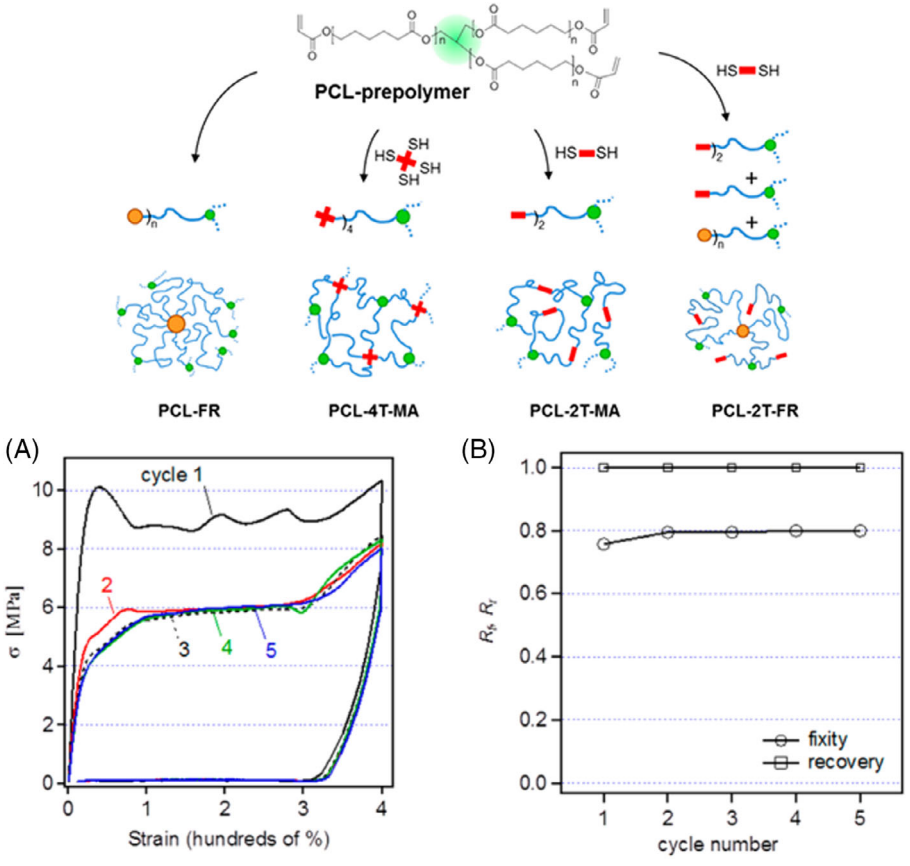

FIGURE 7 Synthesis of semicrystalline network elastomers with different network structures (top); trifunctional cross-links originating from the prepolymer (green), multifunctional cross-links from radical polymerization of acrylate end-groups (orange), and bifunctional and tetrafunctional crosslinks from thiol−acrylate coupling with multifunctional thiol reagents (red). Shape memory performance of PCL networks (bottom); (A) shape memory cycle and (B) shape memory properties with a function of cycle number. Reproduced with permission from Lewis et al.[135]

4 | LIQUID CRYSTALLINE ELASTOMERS

Liquid crystalline elastomers (LCEs) form another class of elastomeric polymers, which have been developed since 1888.[141,142] These elastomers have been used as stimuli-responsive materials due to their ability to reverse shapes in response to external stimuli such as heat and UV.[143,144] This class of polymeric materials has gained attention to promote shape memory effects due to its suitable molecular structure and distinctive transition temperatures.[145,146] The molecular structure of LCEs naturally contains both mesogens (rigid phase) and flexible tails (soft phase).[147,148] The optimal ratio between these two phases plays a significant role in the conformation of LCEs, which enables shape memory behaviors.

Distinctive transition temperatures (T_{tran}) of LCEs play an essential role as a switching point in shape deformation and recovery. Typically, LCEs contain several phase transitions over a well-defined temperature range, that is, a transformation from solid crystal-to-liquid-crystal (SLC) state followed by liquid-crystal-to-isotropic (LCI) state.[25] In a liquid crystal state or mesophase, the molecular chains of LCEs can align differently, resulting in a variety of orientational orders of mesogens. This orientational order can be classified as nematic, smectic A, smectic C, and cholesteric or columnar, as described in.[144,148–152] Among these, smectic and nematic classes of LCEs have been synthesized to promote shape memory behaviors.[153,154] Additionally, these polymeric materials dominate many underlying properties, including electrical, mechanical, magnetic, and anisotropic optical properties upon specific applications.[155]

In last few decades, many research groups have studied shape memory characteristics of various types of LCEs, for instance, p-bis(2,-3-epoxypropoxy)-α-methylstilbene (DOMS),[156,157] polyurethane,[26,158] hydroquinone based hydrogels,[159] siloxane,[160,161] 4-methoxyphenyl 4′-(3-butenyloxy)benzoate attached to poly(methylhydrosiloxane),[162] and diacrylate reactive mesogens.[25]

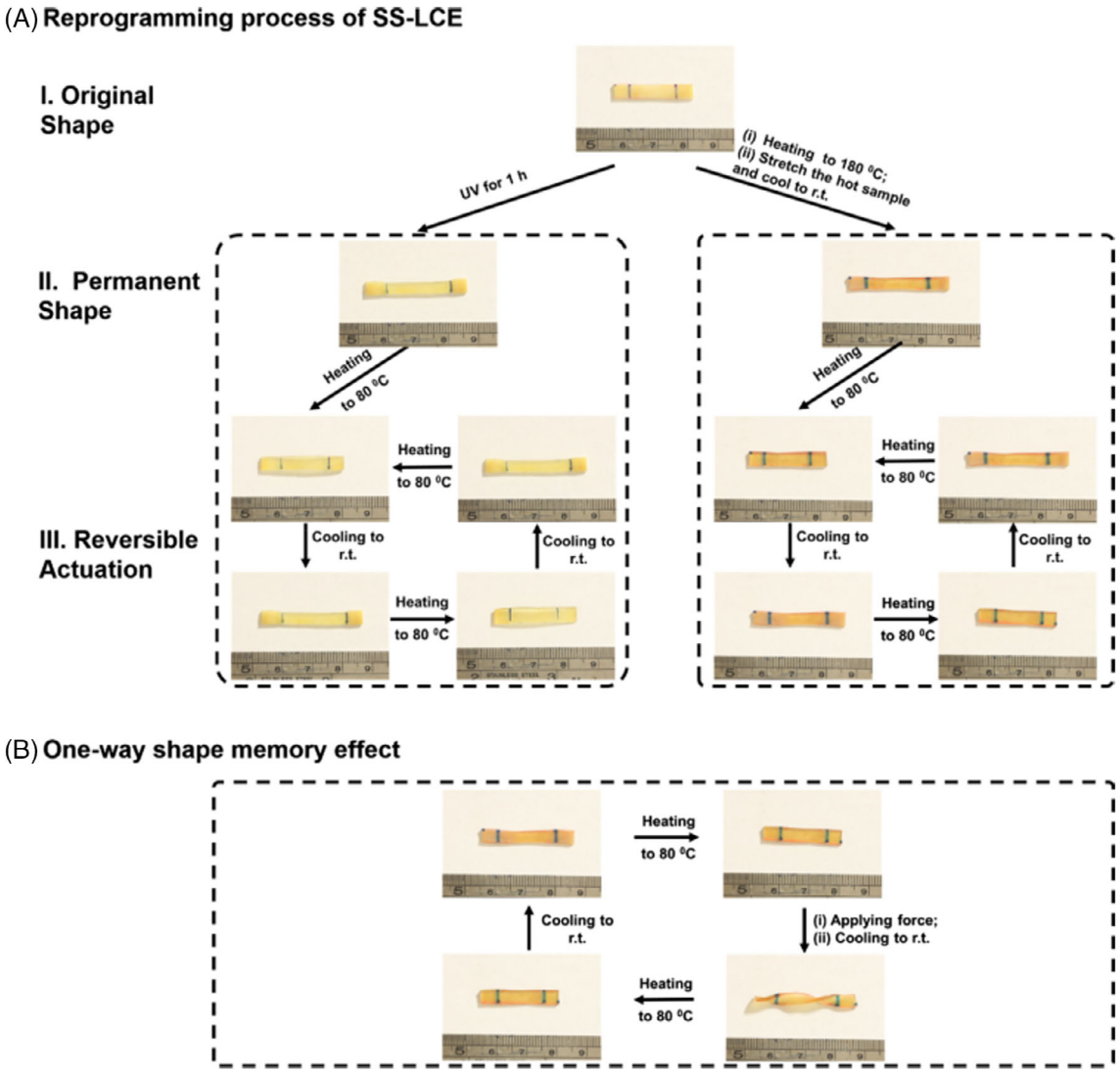

FIGURE 8 Image demonstration of reprogrammability property of the SS-LCE specimen with various stimulation of UV irradiation or heating to 180°C. The specimens exhibited a reversible actuation behavior upon the heating/cooling process (A). The one-way shape memory effect of monodomain LCE sample (B). Reproduced with permission from Wang et al.[163]

Recently, Wang et al.[163] have studied the reprogramming effect of LCEs, which was synthesized by diacrylate mesogen (RM257). Disulfide metathesis was utilized to establish an LCE network via a two-step polymerization using thermal curing and UV irradiation. The LCE samples possessed re-programmability when they were stimulated by heat and UV. The specimen was heated and stretched at 180°C for 10 min and eventually cooled down to room temperature to maintain the stretched samples to formulate an initial shape before a reprogramming process. The specimens were also placed under UV illumination for 1 h during a stretching step to provide UV stimulus. This elastomeric system has proceeded in the following shape memory cycle: the specimen was heated to 80°C while exerting external torque followed by cooling down to ambient temperature and reheating to 80°C. The process of reprogramming and shape memory indicated excellent shape deformation, maintaining, and recovery, as illustrated in Figure 8.[163] In this regard, disulfide bonds performed an essential role in the reprogramming process between polydomain (before deformation) and monodomain (after deformation) states.

LCE with shape memory characteristics was also studied by Li et al.[164] They synthesized LCE-based epoxy using azobenzene and sebacic acid as curing agents. A ring-opening/transesterification catalyst was required for a polymerization process with a step-curing at 170°C for 1 h and 200°C for 3 h. The box-shaped sample exhibited triple shape memory behaviors when processing at transition temperatures, for example, $T_g \sim 80$°C and isotropic temperature (T_i) ~140°C. In a shape memory process, the sample was heated to above its T_i and flattened upon cooling to 85°C to adopt the first temporary shape. Subsequently, it was folded at 85°C to deform to the second temporary shape and cooled down to room temperature. In the recovery process, it was reheated to the abovementioned temperatures to return to the first temporary shape and the permanent shape.

5 | ADVANCED TECHNOLOGIES FOR DESIGNING SMEs

5.1 | 3D and 4D printing

Additive manufacturing (AM) represents a class of contemporary technologies involving materials science, engineering, and technology. AM has been extensively used for constructing physical components or structures by employing virtual 3D computer models.[165,166] The layer-by-layer manufacturing method is typically utilized in AM,[167,168] which has many advantages in terms of fast creation, convenient access, cost-effectiveness, creative design, and geometry customization.[169] The AM technology has been used with a wide range of materials, including bio and synthetic polymers for biomedical devices and tissue engineering, complex geometry in large-scale concrete structures, metals, and ceramic implants.[170–174] 3D printing also allows the use in a field of smart elastomeric materials such as shape memory, self-healing, and other stimuli-responsible functionalities. Fused deposition modeling (FDM) and direct ink writing (DIW) are two commonly used extrusion-based 3D printing techniques to fabricate elastomeric materials at a low cost. Often, the printable elastomers should meet some specific characteristics for successfully creating complex geometries. These include their highly thixotropic or shear-thinning behaviors, suitable rheological properties, shear-dependent viscosity, and sufficient mechanical strength after extrusion to prevent delamination.[175] Many other classes of AM methods have also been developed to generate 3D structural polymeric materials as reported in the literature, for example, by Ngo et al.[167] and Wong et al.[176]. However, this review only highlights 3D and 4D printing techniques that are employed to create SMEs.

Wang et al.[177] have utilized fused deposition modeling (FDM) or fused filament fabrication (FFF) to 3D-print water-based biodegradable polyurethane SME for use as bone scaffolds. This printing technique utilizes a continuous filament fed through a heated printing head. In their work, to make the 3D printing ink, polyethylene oxide (PEO) was first dissolved in water (10% w/w). It was then blended with PU (PEO/PU) in a final weight ratio of 24:76 in order to increase the viscosity. In a comparison, gelatin type A was dissolved in water (7.7% w/w) and then mixed with PU (gelatin/PU) in a final weight ratio of 15:85. 500 ppm of superparamagnetic iron oxide nanoparticles (SPIO NPs) was further added to the ink mix to promote osteogenic induction and shape fixity. The feedstock was extruded through a nozzle with a diameter of 210 μm under the variable pressure of 40 kPa to 250 kPa.[177] The 3D-printing process and printed scaffold samples are shown in Figure 9. The results demonstrated that R_f values of the utilized elastomers were in the range of 85.2% to 100%, and their R_r values were in the range of 73.9% to 89.8%.

Direct ink writing (DIW) or robocasting is another 3D printing technique that has been utilized to manufacture polymeric materials. This method is also based on the extrusion procedure under ambient conditions.[178] The 3D-printing ink for DIW must be in a viscous liquid phase, which can be dispensed out of the nozzle under controlled flow rates. It is deposited along a digitally defined platform to construct the 3D structure.[179,180] This technique can potentially print many types of polymeric ink materials, such as colloidal suspension, hydrogels, thermosetting polymers, and fugitive inks. Often, the polymeric ink requires UV irradiation for photo-polymerization to completely solidify the printed samples for use as SMEs.[181,182]

Davidson et al.[183] printed LCEs by using a high operating temperature (HOT)-DIW technique, as depicted in Figure 10. The LCE ink contained an excess of a difunctional mesogen (RM82) with a 50:50 mixture of ethylene dioxydithane thiol (EDDT) and allyl dithiol (ADT). Bis-acylphosphine oxide (BAPO) and dimethoxy phenyl acetophenone (DMPA)-based photo-initiators were also added to create a bond exchange under exposure to UV light with a wavelength of 400–420 nm. The mechanism of this bond exchange reaction is also shown in Figure 10. The LCE ink with dynamic bonds was printed at 60°C with a print speed of 12 mm/s. This printing temperature implied that the LCE was in its liquid crystal state (nematic-isotropic temperature, T_{NI}, of 90°C) and possessed shear thinning behavior. The ink rapidly transformed into a solid-like response upon printing onto a glass platform at room temperature. The sample was eventually photo-crosslinked with a UV wavelength of 400–500 nm for post-curing.[183]

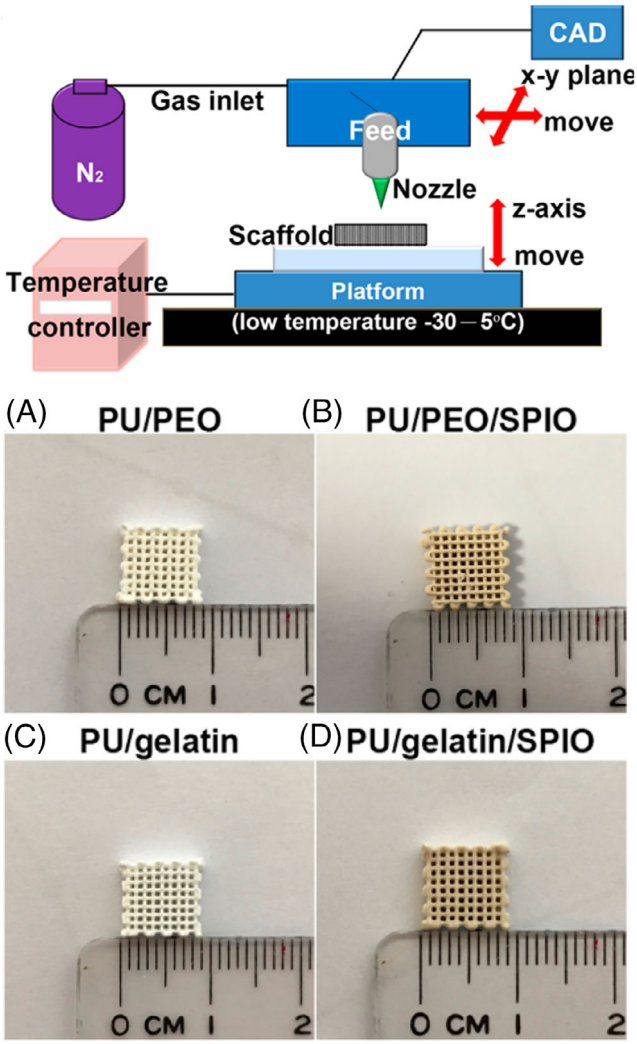

FIGURE 9 An establishment of 3D-printing shape memory scaffolds using a low-temperature fuse deposition manufacturing (LFDM) platform. The platform is set at −30°C for PU/PEO ink and 5°C for PU/gelatin ink (top). Structures of 3D-printed scaffolds with varying chemical compositions (bottom). Reproduced with permission from Wang et al.[177]

In addition, to create dynamic bond-exchange-enabled locked-in states, LCE strips were printed by using a 250-μm nozzle. In Figure 11, the LCE strip samples are optically transparent because of the achieved alignment of liquid crystalline domains via the printing process. Actuation behavior and shape recovery of LCE strips were investigated above T_{NI}, as depicted in Figure 11A. A photomask was placed on the strips to block UV transmission in masked and unmasked regions selectively. The LCE strips show alternating opaque locked-in regions and clear shape recovered regions. Figure 11B, C exhibit the reversibility of heterogeneously alternating LCE strips, synthesized with and without DCBs, when stimulated by heat and UV exposure. Moreover, unbiased linear actuation of these strips occurs over a temperature range of 50 to 125°C. The LCE strips were then deformed by stretching around 50% along the print path and expanding about 50% perpendicular to the print path. A reversible actuation can proceed at least 20 cycles between 25°C and 135°C.[183]

A similar SME system was explored by Kotikian et al.[184] Diacrylate LCEs were printed as bilayers consisting of a 100 μm thick H-shaped layer as the top layer and a square-shaped layer with a thickness of 100 μm and area of 12 mm × 12 mm as the bottom layer. The sample was patterned on a glass substrate using a nozzle with the diameter of 250 μm and a print speed of 4 mm/s at 50°C. The H-shaped layer contained an array of LCE filaments, where it is printed in a meander line pattern by making a 90° angle with the horizontal print path. On the other hand, the square-shaped layer was printed by making a 45° diagonal angle with the horizontal print path. In their results, the repeatable actuation contraction was 43.6% ± 6.7% along with the print direction and the average expansion was 29.8% ± 5.9%. The actuator samples can handle up to 100 cycles. The actuation and relaxation to the original dimensions occurred at 180 s and 210 s, respectively.

Infill percentage and print orientation are other parameters that play a vital role in printing shape memory materials. Villacres et al.[185] demonstrated that infill percentage and print orientation significantly affect the shape recovery (R_r) and mechanical properties of thermoplastic polyurethane (TPU). In their work, the reduction of infill percentage from 100% to 50% increased the recovery speed by 25.7%. However, the recovery force decreased from 457.6 N to 183.7 N. Infill printing angles of 0° and 90° increased the recovery speed from 31.2% to 34.6%. The printing directions of 30°, 60°, and 90° increased mechanical properties of the samples three folds when 100% infill was applied.

Four-dimensional (4D) printing is another AM technology that uses the same techniques like 3D printing through a virtual computer model of materials. However, a time transformation dimension is added to the system.[186,187] This technology has been developed to help overcome the limitations of the static microstructures created by conventional 3D printing. FDM and DIW are the techniques that are commonly used to print the 4D samples and are often combined with a UV light, in two steps, for curing the printed samples via photopolymerization. 4D printing has many advantages in sample printability, such as enhancing capabilities of printed products, enabling new applications using adaptive products, improving manufacturing efficiency, and reducing processing costs and carbon footprint.[188]

Recently, 4D-printed braided tube preforms from PLA filament were manufactured using the FDM technique as shown in Figure 12A,B.[189] The products were designed by software and printed at a temperature of 200°C with a printing speed of 40 mm/s and a controlled layer thickness of 0.2 mm. The braided composite samples were also created by adding carbon nanotube (CNT) to polylactic acid (PLA) to improve their shape memory effects. A camera recorded the shape memory behavior of the 4D printed composites during a well-defined temperature change. Figure 12C–E illustrates the shape recovery behavior and recovery time of a 4D-printed composite-based CNT/PLA with a braiding angle of 30° at a temperature of 70°C. The results also indicated that adding CNT to the PLA matrix increased the recovery force by up to 144%.[189] Therefore, 4D

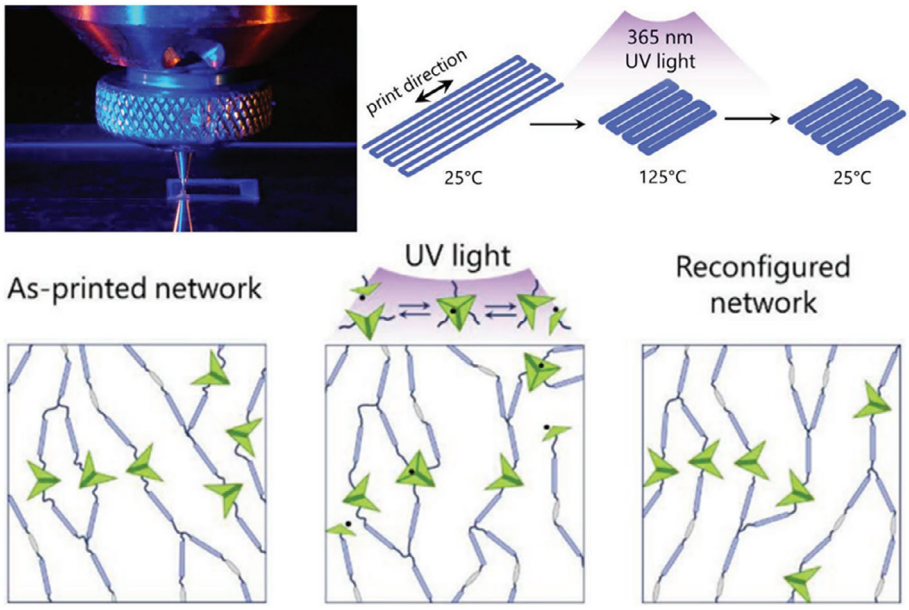

FIGURE 10 HOT-DIW: extruding the liquid crystalline elastomers (LCE) ink with blue light and in situ photo-crosslinking (top), the arrangement of LCE structure (bottom): after printing (left), heating above the T_{NI} (middle), after network reconfiguration into a locked-in state (right). Reproduced from with permission Davidson et al.[183]

printing is highly effective in architecture design and control, hence can be adapted to produce samples in shape memory applications.[190]

5.2 | Machine learning

Machine learning (ML) is a sub-field of artificial intelligence (AI) based on the concept that machines can learn from data, categorize outlines, and make decisions with minimal human interference. This AI technology first appears in the 1950s and is developed to model complex relationships between given observable inputs and outputs. The inputs can be used to predict the desired outputs through a hypothesized mathematical model that is learned by processing the available data and maximizing a problem-dependent performance criterion.[191] In this regard, ML is suitable for advanced modeling and inverse design due to offering several advantages, for example, automated identification of patterns and trends, continuous development, and handling multi-dimensional and diverse data.[192,193] Currently, ML is utilized in many industries, such as financial services, health care, government, oil and gas, transportation, and material science.

ML-assisted discovery of a novel polymeric system with shape memory characteristics has been investigated by Yan et al[194] A dual-convolutional neural network framework based on BigSMILES linear notion[195] and a dataset augmentation method were utilized to encode a polymeric structure as a computer code. This two-step encoding procedure is shown in Figure 13. This novel ML-based method successfully predicts improved recovery stress of epoxy-based SMPs by converting 4459 samples of new SMPs space. It analyzed and separated 14 regularly unknown shape memory systems with higher recovery stress than the well-known systems, as depicted in Figure 14. The success of such methods highlights the potential for discovering novel SMPs with targeted recovery stress using a small training dataset as well as predicting other desired characteristics such as T_g via trial and error.

Dutta et al.[196] have proposed an ML-assisted method to develop novel PU film-based SMPs. They use computer vision and ML techniques for advanced manufacturing material modeling. The proposed method can rapidly characterize novel materials through a combination of experimental results and predictive modeling. The presented modeling workflow delivers an accuracy of 90%, sensitivity of 92%, and specificity of 94% in predicting the recovery behavior of PU films.

Overall, ML-assisted design combined with 3D and 4D printing is a powerful tool for predicting the target properties, inverse design, and modeling the advanced geometry of shape memory materials.[197,198] However, the main challenge with respect to processing SMEs through 3D/4D printing is the selection of suitable materials considering their underlying properties such as rigidity and stiffness, surface quality, dimensional integrity, degradation, and void generation.[199] These properties can affect the adoption of novel SME-related technologies in various engineering applications. The size and the resolution of the printed samples are the other challenges in the conformation design.[199] The SMEs are currently produced in small sizes due to the limitations of the current 3D printers. The major challenges of developing SMEs through ML are the intractability of feature identification, shortage of experimental data for some underlying properties, and lack of multi-length scale structural information.[194] These challenges are currently tackled via several methods with varying degrees of success. To overcome the main challenges surrounding the combined use of ML and 3D/4D printing technologies in SME-related applications, one can consider tailoring the molecular structure of the SMEs to the particular application while taking into account the correlation of the microstructure with relevant processing parameters. Such approaches can ultimately lead to developing novel 3D/4D printing platforms and the associated software and hardware.

6 | APPLICATIONS OF SMEs

SMEs have been synthesized with their microstructures designed to suit specific applications. The composite systems of SMEs are also

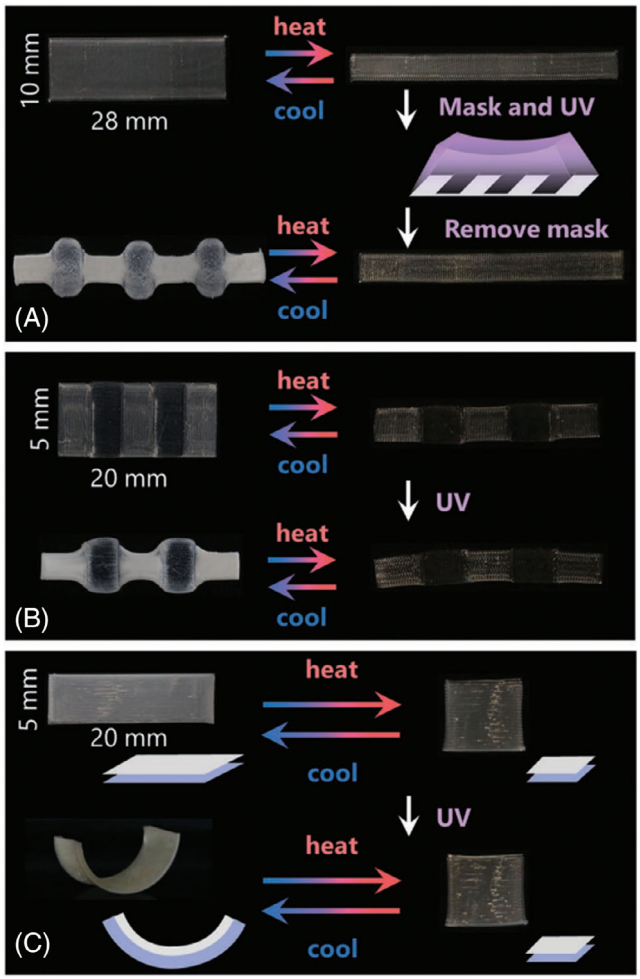

FIGURE 11 Schematics of the methods used for creating locally reconfigured and heterogeneous liquid crystalline elastomers (LCE) structures; (A) locally controlled network reconfiguration by using photolithography, (B) heterogeneous alternating strip of LCE inks with and without dynamic bonds, (C) heterogeneous printed bilayer transitions from linear actuation to bending actuation after high-temperature UV exposure. Reproduced with permission from Davidson et al.[183]

developed to enhance their thermal properties, mechanical strength and modulus, and recovery stress. Improvement of these intrinsic properties can broaden the shape memory applications of SMEs. Currently, SMEs find applications in biomedical devices, soft robotics, drug-releasing agents, and biomedical engineering. Moreover, SMEs are increasingly utilized in industrial engineering applications, for example, self-folding materials, wearable devices, textiles, and vibration damping tools.

6.1 | Biomedical devices and biomaterials

Recently, the vascular LCE-based artificial muscle (VLAM) has been designed and manufactured including an internal fluidic channel.[200] Hot or cold water is injected into the channel to heat up or cool down the device and achieve fast-responsive actuation and recovery. Due to the internal temperature control via heating or cooling, VLAM indicates a strong actuating potential with a wide range of ambient temperatures. For an actuation and recovery process, as depicted in Figure 15, hot water with a temperature of 95°C is injected into the internal fluidic channel. VLAM is then stressed to 40% of its initial length by assigning a weight of 100 g. Cold water at room temperature is eventually injected into the channel to help the device recover its original length. The VLAM actuation demonstrates a recovery process within 10 s when it is stimulated with water, which is faster than with other triggers, such as light or air.

Another distinct example of shape-memory materials for such applications is the poly(ether-ester-urethane)s (SMPEEUs) based on poly(ether-ester) (PECL) and aliphatic diurethane diisocyanate (HBH).[201] This elastomeric system contains many properties of interest for medical device applications including cytocompatibility and nontoxic degradability. Shape memory properties can be measured by a fold-deploy shape memory test when folding with a fixed angle of 180° in water and at body temperature. The results of SMPEEUs revealed that R_f was up to 99.5%, R_r was approximately 99.8%, recovery time was 3.9 s, and shape memory cycle was up to seven times.

Elastomeric materials have also been utilized in biomedical applications such as biomaterial design and tissue engineering. Worch et al.[202] have developed a biocompatible elastomeric polyamide with shape memory properties to be used in long-term implants. They have also studied high trans samples with 67% trans and high cis samples with 86% cis for their hydrolytic stability and water uptake behaviors in relation to biocompatibility and shape memory properties. These samples exhibited minimal degradation and swelling, attesting to the hydrolytic stability of this class of polymers. The favorable shape memory behaviors of these materials can usher a minimally invasive route to implantation by helping decrease the material footprint during surgical treatments. These behaviors can also improve the resilience of implants against deformation or damage. In shape memory testing, these elastomeric materials indicated excellent R_f and R_r values of 99% and 100%, respectively, when stimulated via a thermomechanical process. Interestingly, the high cis and high trans samples exhibited different recovery behaviors. The high cis samples were likely to recover when reaching T_g, while the high trans samples recovered at temperatures higher than T_g (e.g., 120°C).

Wang et al.[203] have developed biocompatible shape memory elastomeric composites based on polyurethane (PU)/zinc oxide (ZnO). These nanocomposites can be used as smart biomaterials with cytocompatibility. Their cytocompatibility was evaluated through cell viability testing. The results confirmed that these materials had weak cytotoxicity and superior cell viability by introducing ZnO nanoparticles in the PU samples. The PU/ZnO also exhibited shape memory characteristics via a thermomechanical process. The R_f values of these samples were 100% at 0°C, and the R_r values were in the range of 83.3% to 93.8% at 37°C. However, the R_r values could approach 100% at 50°C.

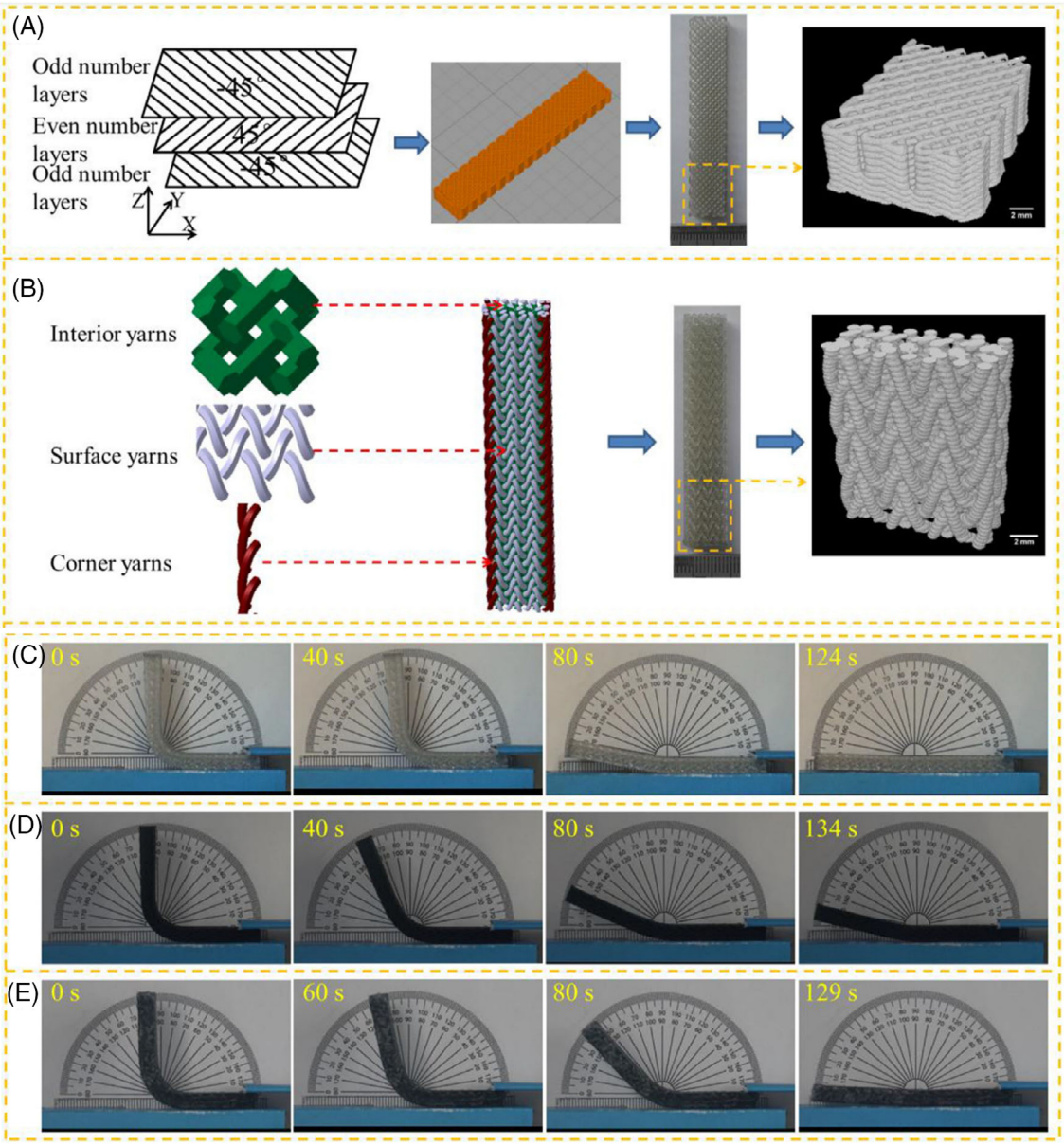

FIGURE 12 Microstructural design and μ-CT imaging of 4D printed preforms; (A) illustration of raster angles, 3D model, as-printed specimen and μ-CT image of the ±45° angle-ply laminated preform with 2 mm scale, (B) representative units of 3D model, as-printed specimen with 2 mm scale, (C) shape recovery processes of 4D-printed PLA braided preform, (D) 4D-printed CNT/PLA braided preform and (E) 4D-printed CNT/PLA braided preform/silicone matrix composite uniformly heated in an oven at 90°C. Reproduced with permission from Liu et al.[189]

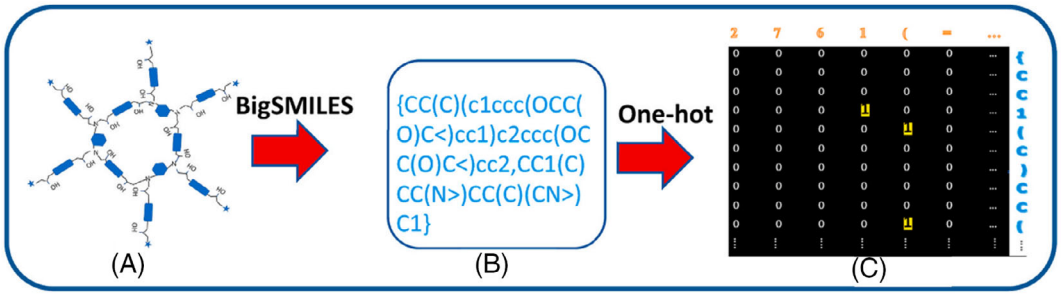

FIGURE 13 A two-step encoding procedure for shape memory polymer; (A) chemical structure, (B) BigSMILES line notation, (C) binary matrix. Reproduced with permission from Yan et al.[194]

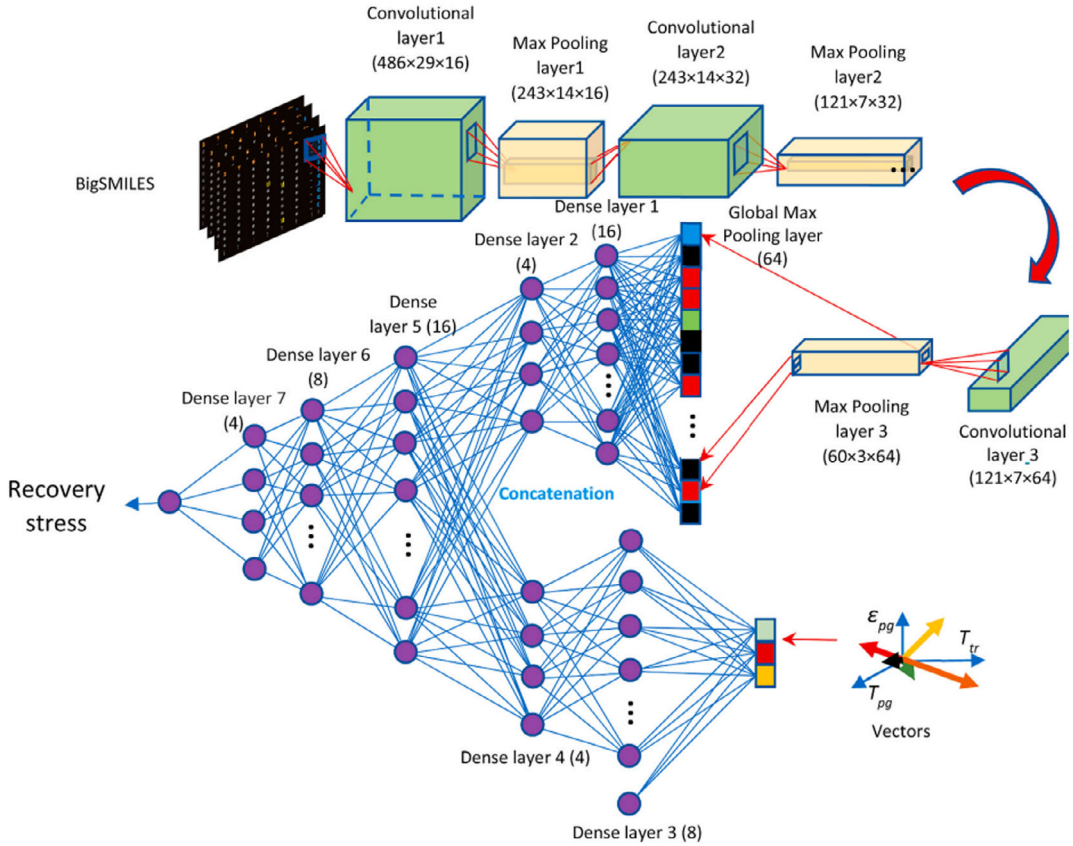

FIGURE 14 The architecture of the neural network model used for recovery stress prediction. Reproduced with permission from Yan et al.[194]

6.2 | Self-folding materials

SMEs can also be used as fold-deploying materials. A specific example is azide/propargyl elastomers, which can fold-deploy at 55°C. This SME can have R_f and R_r values up to 97%. Furthermore, it can recover to the original shape in 12 s and can repeat a shape memory process for up to 5 cycles. Figure 16 illustrates the shape memory behavior of a complicated butterfly structure made of azide/propargyl elastomers, which is constructed to explore its self-folding behavior.[204] In another work, a self-folding box is produced using liquid crystalline polystyrene (PS) bilayers.[205] This LCE can be given temporary shapes through manual stress, for example, curling, twisting, and four-arm folding, as depicted in Figure 16. The shape memory process can be undertaken when the temperature changes. For instance, the four-arm sample can curl upward and relax when stimulated by heat. This behavior can be developed for other planar SMEs, which results in leaf-closing functions.

6.3 | Smart textiles

LCEs based on reactive mesogens with shape memory properties can also be utilized to produce smart textiles through adopting a traditional loom weaving procedure together with standard cotton fibers.[206] The LCEs are typically combined with cotton in the weave direction to induce shape memory features in woven textile. Figure 17 illustrates a textile sample that resembles an original woven textile with two separate parts. It is then activated at 80°C, making LCE fibers to shrink and create pores in the fabric. The LCE fibers expand upon cooling and the textile recovers its initial form.

Sewing LCE fibers into typical cotton can also fabricate smart shirts with shape memory effects.[207] The resultant clothing is initially a barrier to efficient heat transfer and evaporation of sweat.[207] When the body or ambient temperature increases, the LCE fibers can shrink and allow pores to open on the shirt. The LCE fibers can expand and return to the initial configuration again when the temperature reduces. Smart textile with shape memory behaviors can also be generated using other elastomeric systems, as reported by Ji et al.[208] and Haines et al.[209]

6.4 | Smart actuators

Smart actuators are intelligent devices that are used in diverse applications such as robotics, automotive, sensors, and biomedicine.[210] They can be produced in the forms of polymers, fluids, shape memory alloys, liquid metals, and ionic polymer–metal composites (IPMCs).[211,212] Among these forms, IPMCs have gained increasing

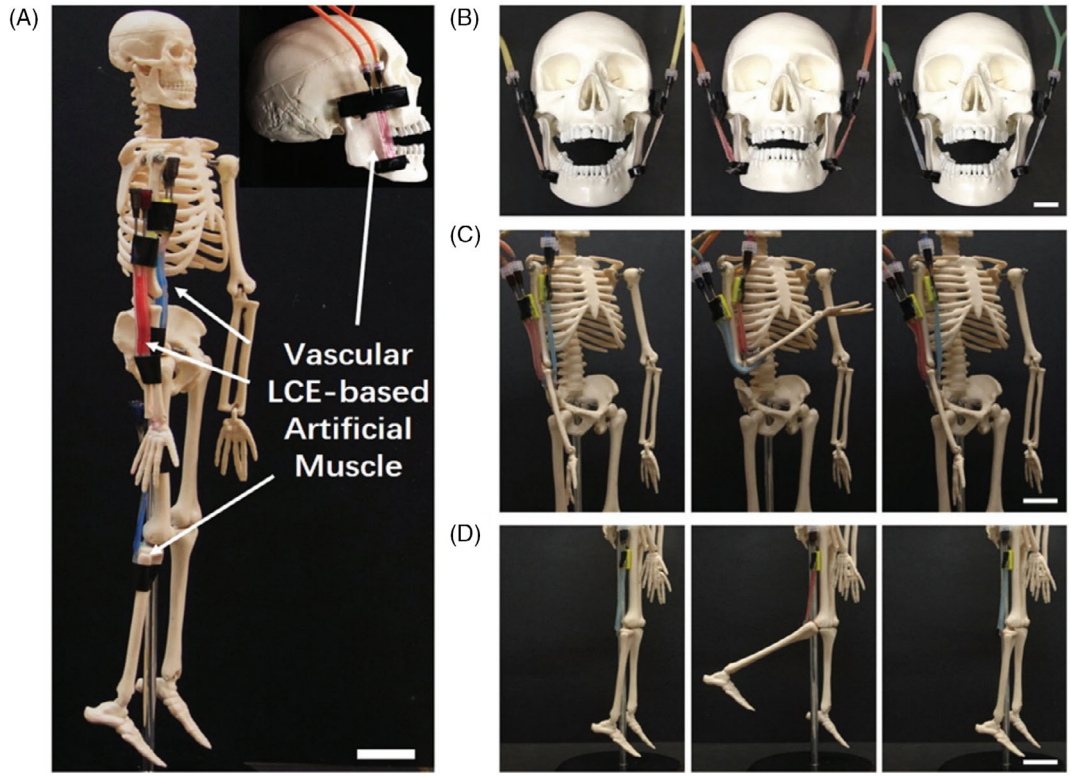

FIGURE 15 Illustration of the usage of vascular LCE-based artificial muscle as biceps, triceps, masseter, and biceps femoris artificial muscles on a human skeleton (A), jaw movement by contracting the artificial masseter muscle (B), lifting an arm by contracting the artificial biceps muscle and relaxing the artificial triceps muscle (C), lifting right lower leg by contracting the artificial biceps femoris muscle (D). Reproduced with permission from He et al.[200]

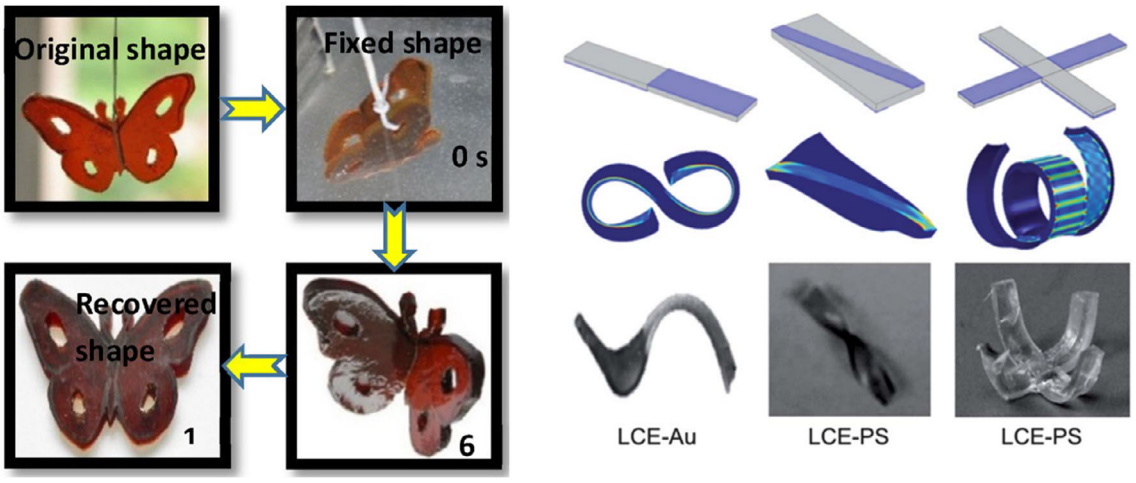

FIGURE 16 Images of butterfly-shaped elastomer exhibiting shape memory behavior (left). Reproduced with permission from Ragin Ramdas et al.[204]. Schematics for patterned liquid crystalline elastomers (LCE)–PS and LCE–Au bilayers for achieving controlled shape changes with finite element method (FEM)-based simulation predictions and experimental samples (right). Reproduced with permission from Agrawal et al.[205]

attention due to their electro-responsiveness in the shape bending process. Typically, IPMCs contain a thin ion-exchange (or ionic-polymer) membrane and two electrodes, making them deform in shape or size when an electric field is applied.[211,213] Furthermore, these materials can function in air, water, and vacuum making them suitable for being used as remotely-controlled actuators in various applications. Swimming and flying robots are prominent examples of the remotely-actuated function, which can be utilized in millimeter or centimeter scales. Slow decomposition, bio-stability, and multi-modal operation are other advantages of utilizing IPMCs.[214] Due to the mechano-

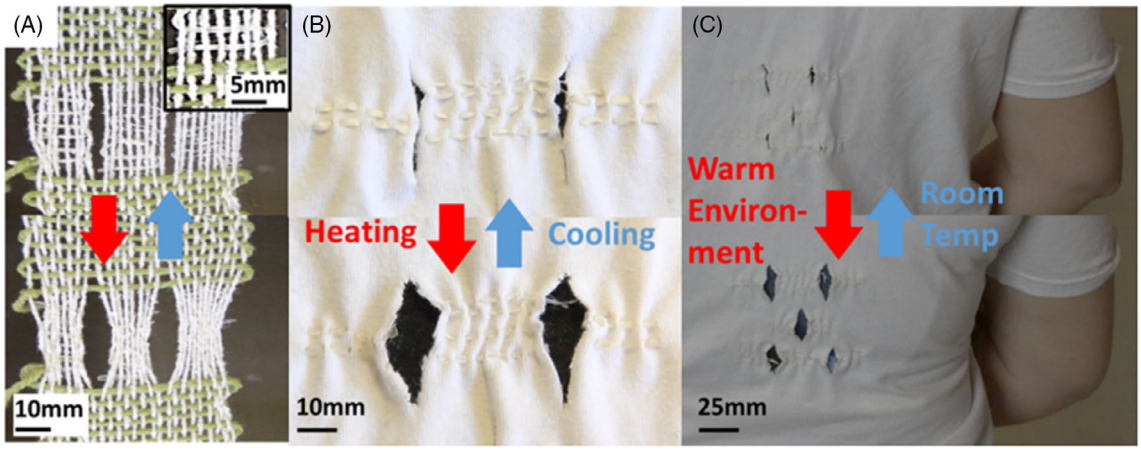

FIGURE 17 (A) liquid crystalline elastomers (LCE) fibers integrated into a smart textile to create pores through temperature change. (B) Sewing of LCE fibers into a cotton shirt generating pores through temperature change. (C) Illustration of the LCE smart shirt exhibiting a change of pore size in various temperatures. Reproduced with permission from Roach et al.[206]

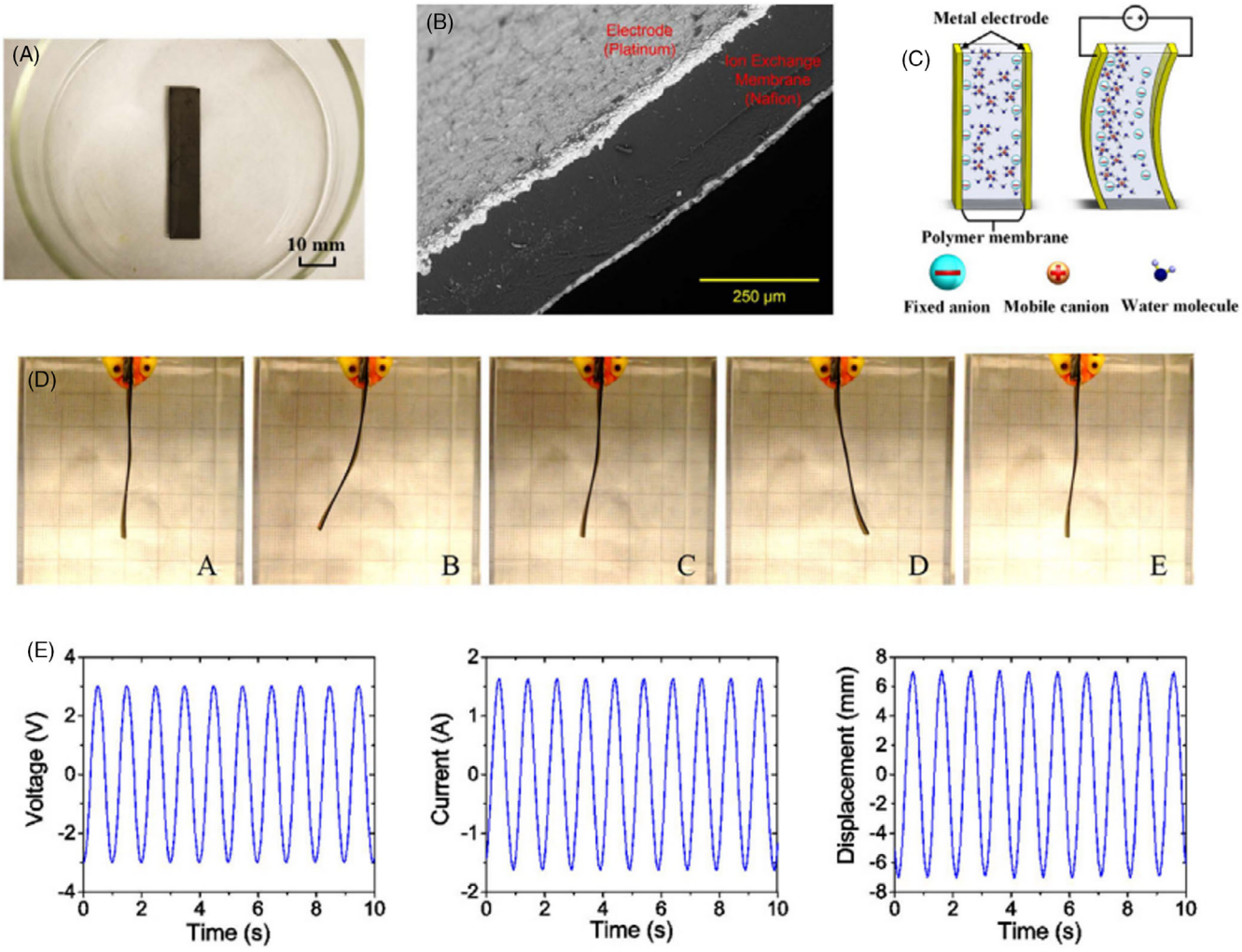

FIGURE 18 Illustration of (A) An ionic polymer–metal composite (IPMC) sample in the evaporating pan; (B) An scanning electron microscope image of a cross-section of IPMC containing the polymer membrane between both sides of the electrodes; (C) A bending deformation mechanism of IMPC when an electric field is applied across this material resulting in the ions to redistribute along with the water molecule; (D) Continuous deformation of IPMC when applying a voltage of 2.6 V with 1 Hz frequency; (E) Input voltage, output current, and displacement of IPMC versus time under the applied input voltage. Reproduced with permission from Shen et al.[215]

electrical and electro-mechanical transaction mechanism of IPMCs, they are also used as shape memory materials.[214,215] The transaction mechanism of IPMCs increases diversity and potential of utilizing external activation in shape memory process unlike the conventional thermal- or UV stimulation of SMEs. Figure 18A–C shows a shape memory IPMC consisting of two or more electrodes sandwiching an ion-conductive polymer material. The specimen can be bent via an electro-mechanical actuation effect when the voltage is applied. The transference of ions and water molecules associated with the electrostatic interactions within the polymer leads to bending deformation, as depicted in Figure 18D–E.

The piezoelectric effect can also be exploited in shape memory applications. This effect is similar to the concept of IPMCs. However, the piezoelectric materials require higher stress than IPMCs to generate electricity due to their high mechanical stiffness. The piezoelectric effect is the result of that electric charge can accumulate in certain polymeric materials when mechanical stress is applied. Conversely, this stress can be generated when an electric field is applied to such materials. These direct and converse piezoelectric effects can benefit the associated shape memory mechanism in terms of applying external force and stimulus in shape fixation and recovery processes.[216,217] To combine shape memory and piezoelectric effects in the same material, Bodkhe and Ermanni[218] have fabricated multifunctional polymeric composites from poly-lactic acid/poly-esteramide (PLA/PEA) while embedding piezoelectric barium titanate nanoparticles. This composite was able to exhibit multiple functionalities, including shape memory effects and piezoelectric sensing, once a 5 N force was applied and the electrodes were connected to both sides of the sample to collect the produce electric charge. This composite had a high recovery rate of approximately 98%. It showed a built-in sensing behavior while withstanding temperature changes from 23 to 100°C over 5000 operation cycles. These multifunctionalities can benefit applications in surveillance and remote sensing where sensors and actuators are deployed at hard-to-access locations.

In addition to IMPCs and piezoelectric materials, other elastomeric composites have also been developed for soft-actuated applications. Kent et al.[219] have explored soft actuation of LCEs with encapsulated liquid metal Joule heaters. In this work, liquid metal operated as stretchable Joule heating elements and transported heat to the LCE samples to induce a shape memory phase transition. These composite materials exhibited shape memory behaviors without the requirement of external heat. However, they could be directly stimulated by an electrical current due to the addition of a liquid metal heater. Pringpromsuk et al.[220] have studied electromechanical actuation of shape memory polyurethane (SMPU) elastomers. The SMPU actuators were combined with a dielectric plasticizer, which were sandwiched between two electrodes: a metal mesh and a foil. Dielectric SMPU actuators demonstrated two-way shape deformation of contraction and expansion over six electric on–off cycles. The largest contraction of these materials reached 6.76% with an electric field of 34.24 V/μm. Figure 19 illustrates the shape recovery behavior of SMPU via thermal activation, which yielded recovery ratios in the range of 94%–99%.

6.5 | Aerospace applications

Utilization of shape memory materials in aerospace is an exciting opportunity and one which also presents enormous challenges in development and control due to the extremely severe space environment, for example, drastically high or low temperature, high vacuum, and UV radiation.[221] These factors can dramatically decrease the effectiveness of shape memory applications of polymeric materials in absence of suitable protective strategies. Therefore, selecting and developing shape memory materials for these applications must be prudent. In particular, UV and electric-field responsive class of SMPs and SMEs may provide a unique approach for remotely controlled actuators suitable for use in a number of functional aerospace application. Arun et al.[222] have developed electro-active polyurethane filled with 2–40 wt% carbon black for aerospace systems. These materials exhibited multi stimuli-responsiveness via the electro-mechanical and thermomechanical actuation processes. Shape recovery of these

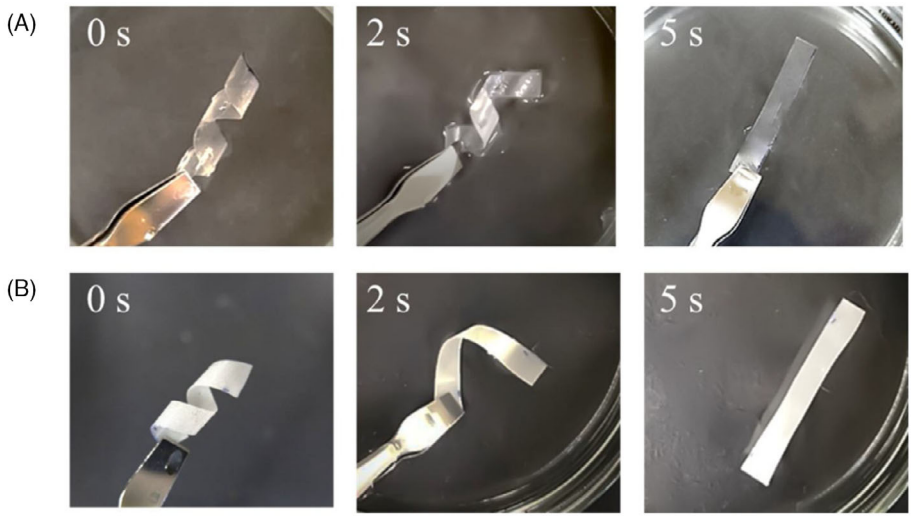

FIGURE 19 Shape recovery of (A) shape memory polyurethane (SMPU) and (B) SMPU with dielectric plasticizer. Reproduced with permission from Pringpromsuk et al.[220]

TABLE 1 The list of potential applications of SMEs

Applications	Materials	Methods for stimulating shape memory effects	Significant properties	Reference
Actuators	Magnetic-particle-embedded Ecoflex	Magnetic field from 100 to 550 mT	Rapid, smooth, and large shape recovery deformation	[225]
	Catechol-Fe^{3+} poly(vinyl alcohol) (PVA) hydrogel	Solvent (water and dimethyl sulfoxide, DMSO), temperatures at 25°C and 55°C, and smearing 0.05 M of $FeCl_3$ solution on the surface	Good shape memory performance under multiple stimulation conditions including temperature, solvent and Fe^{3+} concentration	[226]
	Metal–ligand bonded butadiene–styrene–vinylpyridine rubber	Temperatures at −10°C and 60°C	Shape fixity and recovery ratio were about 80% and 100%	[227]
	Poly(hydrogenmethylsiloxane) (PHMS)	Low-pressure ultraviolet (LPUV) irradiation with an intensity of 50 mW/cm^3 at 120°C	Ability to deform and recover shape upon UV irradiation	[228]
	Liquid crystalline elastomer based 2,6-bisbenzimidazolylpyridine (Bip)	Temperatures at 25°C and 100°C, Solvent (1 mM of $Fe(OTf)_2$), UV light with an intensity of approximately 500 mW/cm^2	99% shape fixity and 98% recovery	[229]
Biodegradable materials	Olefin block copolymer/poly(E-caprolactone) (OBC/PCL)	Temperatures at 30 and 65°C	Shape fixity and shape recovery were in the range of 60% to 100% and 90% to 100%, respectively	[230]
Biocompatible materials	Unsaturated polyurethanes	Temperatures at −35 and 50°C	~98.5% shape fixity and ~90% shape recovery	[231]
Bone tissue engineering	Polyurethane	Temperatures at 25 and 50°C, and soaking in water at 37 and 50°C	Closed to 100% shape fixity and shape recovery and fast recovery time within 6s	[177]
Medical devices	Poly(lactic acid) elastomer (PLAE) and PLA/PLAE	Temperatures at 40 and 75°C	Shape fixity and recovery rate were approximately 97% and 80%, respectively	[208]
	Poly(lactic acid)/polyamide elastomer (PLA/PAE)	Keeping in water bath at room temperature and 80°C	Shape recovery was in the range of 70% to 99%	[232]
	Poly(ether-ester-urethane)s (PEEUs)	Immersing in water bath at 0 and 37.5°C	Excellent recovery ratio of 99.8% and a recovery time of 3.9 s at body temperature	[201]
	Linear polyurethanes (ISO-PUs)	Temperatures at 25 and 60°C	Shape fixity ratio of up to 99.6% and a recovery ratio of up to 90.2%	[233]
	Biobased polyester elastomer	Temperatures at 20 and 90°C	Shape fixity and recovery ratio were about 80% and 95%	[234]
Morphing structure	Olefin block copolymer/silicone elastomeric blends	Temperatures at 20 and 140°C	Up to 84.3% and 97.7% of shape fixity and shape recovery	[5]
Scaffolds	Polyhydroxyalkanoate (PHA)-based polyurethane (PHP)	Temperatures at −4 and 70°C	High shape fixing (>99%) and shape recovery ratio (>90%)	[235]
Sensors	mPEG-acrylate and acryloylmropholine (ACMO) grafted with oligo poly(ethylene glycol)	Temperatures at 0 and 37°C	Recovery within 4 min at 37°C and high self-healing rate	[236]
Soft robotics	Azobenzene-containing polymer network (APN)	UV light from 10 to 50 mW/cm^2	Shape recovery ratio of 85%, and the fixity ratio from 16% to 70%	[237]
Soft tissue repair	Poly(glycerol dodecanoate)	Temperatures at 25 and 145°C and held in water bath at 37°C	Shape recovery nearly 100% and high recovery rate up to 6 mm/s	[238]
Textiles	1,4-bis-[4-(3-acryloyloxypropyloxy) benzoyloxy]-2-methylbenzene (RM 257) based liquid crystalline elastomers	Temperatures at 25 and 120°C	Excellent two-way shape memory textile, modulus of 2 MPa, 51% actuation strain, and a failure strain of 100%	[206]

TABLE 1 (Continued)

Applications	Materials	Methods for stimulating shape memory effects	Significant properties	Reference
	Polyamide12/polyolefin elastomer blends compatibilized by glycidylisobutyl polyhedral oligomericsilsesquioxane (G-POSS)	Temperatures at 0 and 70°C	Up to 95% of shape fixity and recovery when adding 15 phr of G-POSS to the elastomer blends	[239]
	Linear poly(caprolactone)s	Temperatures at 25 and 60°C	Excellent shape fixity and shape recovery up to 99%	[240]
Vibration damping	Nano fly ash (NFA) filled linseed oil elastomer composites	Deforming at $T_g + 50$°C and quenching in water at room temperature for fixing	100% shape recovery, and the shape recovery time improves with increasing of the content of NFA filler	[241]
Wearable devices	Biomass bifunctional polyamide elastomers (BbPEs)	Temperatures at 0 and 60°C	Shape recovery reaches 95% in 5 min. The recovery efficiency is 88.9%	[242]

materials was in the range of 94%–98% once actuated by these stimuli. They could maintain these properties up to eight shape memory cycles. Furthermore, the utilization of carbon black improved UV stability by absorbing and dissipating as heat energy without affecting the underlying properties of these materials.

Shape memory polymeric systems have also been exploited in space deployable structures. Hinges are one of the key deployable features commonly used in aerospace industries. However, the traditional design of these devices experienced some troubles such as shock effect, recovery precision, elastic strain energy distribution, and inflation.[221,223] Many research groups have developed more complex and higher-level designs to overcome these limitations and increase working efficiency and performance. Shape memory polymeric composite (SMPC) hinges have been developed and become a viable candidate for this purpose. Recently, Dao et al.[223] have fabricated SMPC hinges by combining carbon-epoxy with SMP resin. These composite materials demonstrated a nearly 100% recovery ratio and fast recovery time at $T_g + 10$°C and $T_g + 20$°C via folding and deploying cycles. The damage evolution of SMPC hinges was also observed by a USB digital microscope and a scanning electron microscope associated with finite element analysis. The results confirmed that these devices could be used up to 12 reconfiguration cycles before complete structural disintegration. Furthermore, Akbari et al.[224] have employed a 4D printing technique to design and fabricate active composite hinges for a morphing wing flap and a deployable structure. The combination of the active hinges and flexible hinges could store elastic strain energy during a programming step and release it during actuation, causing an increase in the recovery force of the materials. The 4D printed flexible hinges could increase a load-bearing capacity in a deployable process thanks to the higher stiffness of the printed structure.

Other potential applications of SMEs are summarized in Table 1 with the details on their utilization, types of elastomeric systems, and key functional characteristics.

7 | SUMMARY AND OUTLOOK

Due to being responsive to several types of external stimuli, SMEs can be employed in a vast array of industrial engineering and biomedical applications. The recent rapid development of SMEs has created opportunities for enhancing their properties according to the requirements of several real-world applications. A study of the chemistry/synthesis methodology of SMEs allows the researchers to improve the understanding of shape memory behaviors. In this review article, dynamic covalent bond (DCB) chemistry of SMEs is discussed in terms of their synthesis, stimuli-responsiveness, and potentials to use shape memory effects in elastomeric systems. DCBs can promote the chemical transformation of the molecular structure during a shape memory process, allowing the reversibility in its mechanism. The underlying mechanism of SMEs is also described based on the thermomechanical characteristics to provide insights into the associated dynamic molecular transformation. In the last decade, SMEs with underlying dynamic covalent bond mechanism have gained attention for increased use in engineering and biomedical applications. These include robotics, remotely actuated systems, biomedical devices, and assembly packaging including those promised for the space industry. Therefore, the variety and facile access to the complex molecular structures through DCBs will expand a preparation of SMEs for future applications.

LCEs are also discussed in detail together with their shape memory characteristics. LCEs possess outstanding properties that can be utilized for shape memory functionality, such as appropriate molecular structure and phase transition among solid crystal, liquid crystal, and isotropic states. A combination of mesogens and flexible tails in polymeric chains of LCEs suits shape memory effects. Moreover, transition temperatures between different states can be used as a thermal trigger in a shape memory process. These characteristics provide LCEs with stimuli-responsive properties and expand the boundaries of synthesis and utilization of SMEs for meeting the current needs of industries.

Advanced manufacturing technology has been introduced in the structural design at the macroscopic level. This technology encompasses several methods to manufacture elastomeric samples in three and four dimensions. Specifically, FDM and DIW methods are extensively used for printing SMEs. AM can increase the independence of geometry design and customization. Moreover, it has many advantages in terms of low cost, ease of processing, and high speed. Infill percentage and print orientation are also essential factors that influence the shape memory and mechanical properties of SMEs. The 4D printing of SMEs can be monitored in engineering applications such as aerospace, automotive, and defense.

ML has emerged as a powerful tool that can be used to design and customize the shape memory characteristics. ML-assisted discovery of novel SMPs with the desired properties is a potential procedure that can be developed with limited experimentation and human interference. Using ML, one can automatically discover novel shape memory materials by screening a large set of trained data (inputs) to identify the desired characteristic (outputs).

To develop future SMEs, 3D and 4D printing AM technologies can be utilized to generate innovative structures with entirely different designs. The printing techniques such as FDM and DIW can be further developed to serve specific use-cases including soft robotics, wearable devices, and aerospace engineering. New SMEs can also be developed for biomedical applications such as artificial organs and biodegradable materials. 3D and 4D printing are likely to bring about breakthroughs in design and manufacturing of SME-based product for practical applications.

ML methods and AM technologies can be utilized for designing shape memory materials. ML and other AI technologies can help discover novel chemical compositions or understand underlying structures of SMEs, which can exhibit desired characteristics and specific inverse design such as shape fixity, shape recovery, and stress recovery. ML-based and data-driven approaches are especially promising in designing SMEs for critical applications such as smart robots. The development of flexible appliances, which can alter their body shape and physical properties, will allow them to adapt to specific task requirements and environmental conditions.

ACKNOWLEDGMENTS

Open access publishing facilitated by Swinburne University of Technology, as part of the Wiley - Swinburne University of Technology agreement via the Council of Australian University Librarians. [Correction added on 26 May 2022, after first online publication: CAUL funding statement has been added.]

CONFLICT OF INTEREST

The authors declare no conflict of interest.

DATA AVAILABILITY STATEMENT

Data sharing not applicable to this article as no datasets were generated or analyzed during the current study.

ORCID

Peerawat Prathumrat https://orcid.org/0000-0001-5283-8145
Mostafa Nikzad https://orcid.org/0000-0003-4631-3427
Elnaz Hajizadeh https://orcid.org/0000-0001-7679-2233

REFERENCES

1. Feldman D. Polymer history. *Des Monomers Polym*. 2008;11:1-15.
2. Ma W, Cross L. An experimental investigation of electromechanical response in a dielectric acrylic elastomer. *Appl Phys A*. 2004;78:1201-1204.
3. Stricher AM, Rinaldi RG, Barrès C, Ganachaud F, Chazeau L. How I met your elastomers: from network topology to mechanical behaviours of conventional silicone materials. *RSC Adv*. 2015;5:53713-53725.
4. Jang J, Park H, Jeong H, et al. Thermoset elastomers covalently crosslinked by hard nanodomains of triblock copolymers derived from carvomenthide and lactide: tunable strength and hydrolytic degradability. *Polym Chem*. 2019;10:1245-1257.
5. Lai S-M, Chen Y-J, Yu B-Y. Preparation and characterization of two-way shape memory olefin block copolymer/silicone elastomeric blends. *J Appl Polym Sci*. 2021;138:51238.
6. Mehrbakhsh E, Rezaei M, Babaie A, Mohammadi A, Mayan Sofla RL. Physical and thermo-mechanical properties of shape memory polyurethane containing reversible chemical cross-links. *J Mech Behav Biomed Mater*. 2021;116:104336.
7. Major Z, Lang RW. Characterization of the fracture behavior of NBR and FKM grade elastomers for oilfield applications. *Eng Fail Anal*. 2010;17:701-711.
8. Liu X, Zhao J, Yang R, Iervolino R, Barbera S. Effect of lubricating oil on thermal aging of nitrile rubber. *Polym Degrad Stab*. 2018;151:136-143.
9. Walter G. Elastomers in the automotive industry. *Rubber Chem Technol*. 1976;49:775-822.
10. Wang R, Zhang J, Kang H, Zhang L. Design, preparation and properties of bio-based elastomer composites aiming at engineering applications. *Compos Sci Technol*. 2016;133:136-156.
11. Kanyanta V, Ivankovic A. Mechanical characterisation of polyurethane elastomer for biomedical applications. *J Mech Behav Biomed Mater*. 2010;3:51-62.
12. Prem N, Schale F, Zimmermann K, Gowda DK, Odenbach S. Synthesis and characterization of the properties of thermosensitive elastomers with thermoplastic and magnetic particles for application in soft robotics. *J Appl Polym Sci*. 2021;138:51296.
13. Bastola AK, Rodriguez N, Behl M, Soffiatti P, Rowe NP, Lendlein A. Cactus-inspired design principles for soft robotics based on 3D printed hydrogel-elastomer systems. *Mater Des*. 2021;202:109515.
14. Wang F, Zhang C, Wan X. Carbon nanotubes-coated conductive elastomer: electrical and near infrared light dual-stimulated shape memory, self-healing, and wearable sensing. *Ind Eng Chem Res*. 2021;60:2954-2961.
15. Feng X, Zhang G, Xu B, Jiang H, Bai Q, Li H. Self-healing elastomer assembly towards three-dimensional shape memory devices. *RSC Adv*. 2015;5:70000-70004.
16. Lu C, Liu Y, Liu X, Wang C, Wang J, Chu F. Sustainable multiple-and multistimulus-shape-memory and Self-healing elastomers with semi-interpenetrating network derived from biomass via bulk radical polymerization. *ACS Sustain Chem Eng*. 2018;6:6527-6535.
17. Xie T. Recent advances in polymer shape memory. *Polymer*. 2011;52:4985-5000.
18. Lendlein A. Progress in actively moving polymers. *J Mater Chem*. 2010;20:3332-3334.
19. Meng Q, Hu J. A review of shape memory polymer composites and blends. *Compos A: Appl Sci Manuf*. 2009;40:1661-1672.
20. Chen J, Su Q, Guo R, et al. A multitasking hydrogel based on double dynamic network with quadruple-stimuli sensitiveness, autonomic self-healing property, and biomimetic adhesion ability. *Macromol Chem Phys*. 2017;218:1700166.
21. Zou W, Dong J, Luo Y, Zhao Q, Xie T. Dynamic covalent polymer networks: from old chemistry to modern day innovations. *Adv Mater*. 2017;29:1606100.
22. Ooi HW, Hafeez S, van Blitterswijk CA, Moroni L, Baker MB. Hydrogels that listen to cells: a review of cell-responsive strategies in

biomaterial design for tissue regeneration. *Mater Horiz*. 2017;4:1020-1040.
23. Huang S, Kong X, Xiong Y, et al. An overview of dynamic covalent bonds in polymer material and their applications. *Eur Polym J*. 2020;141:110094.
24. Zhang ZP, Rong MZ, Zhang MQ. Polymer engineering based on reversible covalent chemistry: a promising innovative pathway towards new materials and new functionalities. *Prog Polym Sci*. 2018;80:39-93.
25. Prathumrat P, Sbarski I, Hajizadeh E, Nikzad M. A comparative study of force fields for predicting shape memory properties of liquid crystalline elastomers using molecular dynamic simulations. *J Appl Phys*. 2021;129:155101.
26. Shen W, Liu J, Du B, et al. Thermal- and light-responsive programmable shape-memory behavior of liquid crystalline polyurethanes with pendant photosensitive groups. *J Mater Chem A*. 2021;9:15087-15094.
27. Guo Y, Shahsavan H, Sitti M. 3D microstructures of liquid crystal networks with programmed voxelated director fields. *Adv Mater*. 2020;32:2002753.
28. Sawamura M, Kawai K, Matsuo Y, Kanie K, Kato T, Nakamura E. Stacking of conical molecules with a fullerene apex into polar columns in crystals and liquid crystals. *Nature*. 2002;419:702-705.
29. Garidel P, Kaconis Y, Heinbockel L, et al. Self-organisation, thermotropic and lyotropic properties of glycolipids related to their biological implications. *Open Biochem J*. 2015;9:49-72.
30. Burke KA, Mather PT. Soft shape memory in main-chain liquid crystalline elastomers. *J Mater Chem*. 2010;20:3449-3457.
31. Guo H, Dai W, Miao Y, Wang Y, Ma D, Xue W. Sustained heparin release actuator achieved from thermal and water activated shape memory hydrogels containing main-chain LC units. *Chem Eng J*. 2018;339:459-467.
32. Miao S, Zhu W, Castro NJ, Leng J, Zhang LG. Four-dimensional printing hierarchy scaffolds with highly biocompatible smart polymers for tissue engineering applications. *Tissue Eng Part C Methods*. 2016;22:952-963.
33. Muth JT, Vogt DM, Truby RL, et al. Embedded 3D printing of strain sensors within highly stretchable elastomers. *Adv Mater*. 2014;26:6307-6312.
34. Pugalendhi A, Ranganathan R, Chandrasekaran M. Effect of process parameters on mechanical properties of VeroBlue material and their optimal selection in PolyJet technology. *Int J Adv Manuf Technol*. 2019;108:1049-1059.
35. Peng B, Yang Y, Ju T, Cavicchi KA. Fused filament fabrication 4D printing of a highly extensible, self-healing, shape memory elastomer based on thermoplastic polymer blends. *ACS Appl Mater Interfaces*. 2021;13:12777-12788.
36. Yuan C, Wang F, Qi B, Ding Z, Rosen DW, Ge Q. 3D printing of multi-material composites with tunable shape memory behavior. *Mater Des*. 2020;193:108785.
37. Samuel AL. Some studies in machine learning using the game of checkers. *IBM J Res Dev*. 2000;44:206-226.
38. Hu X, Wang J, Wang Y, et al. Two-way design of alloys for advanced ultra supercritical plants based on machine learning. *Comput Mater Sci*. 2018;155:331-339.
39. Liu S, Kappes BB, Amin-ahmadi B, Benafan O, Zhang X, Stebner AP. Physics-informed machine learning for composition–process–property design: shape memory alloy demonstration. *Appl Mater Today*. 2021;22:100898.
40. Rodemerck U, Baerns M, Holena M, Wolf D. Application of a genetic algorithm and a neural network for the discovery and optimization of new solid catalytic materials. *Appl Surf Sci*. 2004;223:168-174.
41. Erden N, Jana SC. Synthesis and characterization of shape-memory polyurethane-polybenzoxazine compounds. *Macromol Chem Phys*. 2013;214:1225-1237.
42. Rousseau IA, Xie T. Shape memory epoxy: composition, structure, properties and shape memory performances. *J Mater Chem*. 2010;20:3431-3441.
43. Prathumrat P, Tiptipakorn S, Rimdusit S. Multiple-shape memory polymers from benzoxazine–urethane copolymers. *Smart Mater Struct*. 2017;26:065025.
44. Zhang S, Bellinger AM, Glettig DL, et al. A pH-responsive supramolecular polymer gel as an enteric elastomer for use in gastric devices. *Nat Mater*. 2015;14:1065-1071.
45. Bai J, Shi Z. Dynamically cross-linked elastomer hybrids with light-induced rapid and efficient self-healing ability and reprogrammable shape memory behavior. *ACS Appl Mater Interfaces*. 2017;9:27213-27222.
46. Yang L, Ouyang P, Chen Y, et al. Tough self-reporting elastomer with NIR induced shape memory effect. *Giant*. 2021;8:100069.
47. Wu T, O'Kelly K, Chen B. Poly(vinyl alcohol) particle-reinforced elastomer composites with water-active shape-memory effects. *Eur Polym J*. 2014;53:230-237.
48. Quitmann D, Gushterov N, Sadowski G, Katzenberg F, Tiller JC. Solvent-sensitive reversible stress-response of shape memory natural rubber. *ACS Appl Mater Interfaces*. 2013;5:3504-3507.
49. McCoul D, Rosset S, Besse N, Shea H. Multifunctional shape memory electrodes for dielectric elastomer actuators enabling high holding force and low-voltage multisegment addressing. *Smart Mater Struct*. 2016;26:025015.
50. Zhang DW, Liu YJ, Leng JS. Magnetic field activation of thermo-responsive shape-memory polymer with embedded Micron sized Ni powder. *Adv Mater Res*. 2010;123-125:995-998.
51. Kalita V, Dzhezherya YI, Cherepov S, et al. Critical bending and shape memory effect in magnetoactive elastomers. *Smart Mater Struct*. 2021;30:025020.
52. Sujithra R, Srinivasan S, Arockiarajan A. Shape recovery studies for coupled deformations in an epoxy based amorphous shape memory polymers. *Polym Test*. 2015;48:1-6.
53. Tekay E. Thermo-responsive shape memory behavior of poly(styrene-b-isoprene-b-styrene)/ethylene-1-octene copolymer thermoplastic elastomer blends. *Polym Adv Technol*. 2021;32:428-438.
54. Dong HQ, Liu LJ, Li YY. Shape-memory behavior of poly(L-lactide)/poly(ε-caprolactone) blends. *Adv Mater Res*. 2011;266:171-174.
55. Hu J, Zhang C, Ji F, Li X, Han J, Wu Y. Revealing the morphological architecture of a shape memory polyurethane by simulation. *Sci Rep*. 2016;6:1-9.
56. Chien YC, Chuang WT, Jeng US, Hsu SH. Preparation, characterization, and mechanism for biodegradable and biocompatible polyurethane shape memory elastomers. *ACS Appl Mater Interfaces*. 2017;9:5419-5429.
57. Salaeh S, Das A, Wießner S. Design and fabrication of thermoplastic elastomer with ionic network: a strategy for good performance and shape memory capability. *Polymer*. 2021;223:123699.
58. Li H, Sivasankarapillai G, McDonald AG. Lignin valorization by forming thermally stimulated shape memory copolymeric elastomers—partially crystalline hyperbranched polymer as crosslinks. *J Appl Polym Sci*. 2014;131:12050–12060.
59. Thakur S, Karak N. Multi-stimuli responsive smart elastomeric hyperbranched polyurethane/reduced graphene oxide nanocomposites. *J Mater Chem A*. 2014;2:14867-14875.
60. Du J, Liu D, Zhang Z, et al. Dual-responsive triple-shape memory polyolefin elastomer/stearic acid composite. *Polymer*. 2017;126:206-210.
61. Chakma P, Konkolewicz D. Dynamic covalent bonds in polymeric materials. *Angew Chem Int Ed*. 2019;58:9682-9695.
62. Robinson LL, Self JL, Fusi AD, et al. Chemical and mechanical tunability of 3D-printed dynamic covalent networks based on boronate esters. *ACS Macro Lett*. 2021;10:857-863.

63. Rekondo A, Martin R, de Luzuriaga AR, et al. Catalyst-free room-temperature self-healing elastomers based on aromatic disulfide metathesis. *Mater Horiz*. 2014;1:237-240.
64. Lai Y, Kuang X, Zhu P, Huang M, Dong X, Wang D. Colorless, transparent, robust, and fast scratch-self-healing elastomers via a phase-locked dynamic bonds design. *Adv Mater*. 2018;30:1802556.
65. Lu YX, Guan Z. Olefin metathesis for effective polymer healing via dynamic exchange of strong carbon–carbon double bonds. *J Am Chem Soc*. 2012;134:14226-14231.
66. Lu YX, Tournilhac F, Leibler L, Guan Z. Making insoluble polymer networks malleable via olefin metathesis. *J Am Chem Soc*. 2012;134:8424-8427.
67. Zheng N, Fang Z, Zou W, Zhao Q, Xie T. Thermoset shape-memory polyurethane with intrinsic plasticity enabled by transcarbamoylation. *Angew Chem Int Ed*. 2016;55:11421-11425.
68. Chen X, Li L, Jin K, Torkelson JM. Reprocessable polyhydroxyurethane networks exhibiting full property recovery and concurrent associative and dissociative dynamic chemistry via transcarbamoylation and reversible cyclic carbonate aminolysis. *Polym Chem*. 2017;8:6349-6355.
69. Zhang YC, Le XX, Lu W, et al. An "off-the-shelf" shape memory hydrogel based on the dynamic borax-diol ester bonds. *Macromol Mater Eng*. 2018;303:1800144.
70. Sanyal A. Diels–Alder cycloaddition-Cycloreversion: a powerful combo in materials design. *Macromol Chem Phys*. 2010;211:1417-1425.
71. Lu X, Fei G, Xia H, Zhao Y. Ultrasound healable shape memory dynamic polymers. *J Mater Chem A*. 2014;2:16051-16060.
72. Jeong HJ, Kim BK. Shape memory hyperbranched polyurethanes via thiol-ene click chemistry. *React Funct Polym*. 2017;116:92-100.
73. Ramdas MR, Kumar KS, Nair CR. Click polymerizations: encouraging route for shape memory polymers. *Mater Lett*. 2016;172:216-221.
74. Fortman DJ, Snyder RL, Sheppard DT, Dichtel WR. Rapidly reprocessable cross-linked polyhydroxyurethanes based on disulfide exchange. *ACS Macro Lett*. 2018;7:1226-1231.
75. Song YX, Rong MZ, Zhang MQ. Improvement of multiple-responsive shape memory effects of wool through increasing the content of disulfide bonds. *Polymer*. 2020;188:122130.
76. Bang E-K, Lista M, Sforazzini G, Sakai N, Matile S. Poly(disulfide)s. *Chem Sci*. 2012;3:1752-1763.
77. Tran PD, Tran TV, Orio M, et al. Coordination polymer structure and revisited hydrogen evolution catalytic mechanism for amorphous molybdenum sulfide. *Nat Mater*. 2016;15:640-646.
78. Zhang L, Chen L, Rowan SJ. Trapping dynamic disulfide bonds in the hard segments of thermoplastic polyurethane elastomers. *Macromol Chem Phys*. 2017;218:1600320.
79. Fairbanks BD, Singh SP, Bowman CN, Anseth KS. Photodegradable, photoadaptable hydrogels via radical-mediated disulfide fragmentation reaction. *Macromolecules*. 2011;44:2444-2450.
80. Zhao D, Liu S, Wu Y, Guan T, Sun N, Ren B. Self-healing UV light-curable resins containing disulfide group: synthesis and application in UV coatings. *Prog Org Coat*. 2019;133:289-298.
81. Michal BT, Jaye CA, Spencer EJ, Rowan SJ. Inherently photohealable and thermal shape-memory polydisulfide networks. *ACS Macro Lett*. 2013;2:694-699.
82. Reyes ML, Troadec T, Rodriguez R, et al. Donor/acceptor-stabilized 1-silaketene: reversible [2+2] cycloaddition with pyridine and evolution by an olefin metathesis reaction. *Chem: Eur J*. 2016;22:10247-10253.
83. Quaglio D, Zappia G, De Paolis E, et al. Olefin metathesis reaction as a locking tool for macrocycle and mechanomolecule construction. *Org Chem Front*. 2018;5:3022-3055.
84. Cheng Z. Catalytic Conversion of Carbon-Containing Compounds into Valuable Chemicals and Fuels. Dissertation, Washington University in St. Louis; 2014.
85. Sues PE, Bukhryakov KV, Schrock RR. Evaluation of several molybdenum and ruthenium catalysts for the metathesis homocoupling of 3-Methyl-1-Butene. *Helv Chim Acta*. 2017;100:e1700181.
86. Chen Y, Abdellatif MM, Nomura K. Olefin metathesis polymerization: some recent developments in the precise polymerizations for synthesis of advanced materials (by ROMP, ADMET). *Tetrahedron*. 2018;74:619-643.
87. Ghashghaee M, Ghambarian M. Initiation of heterogeneous Schrock-type Mo and W oxide metathesis catalysts: a quantum thermochemical study. *Comput Mater Sci*. 2018;155:197-208.
88. Buchmeiser MR. Molybdenum imido, tungsten imido and tungsten oxo alkylidene N-heterocyclic carbene olefin metathesis catalysts. *Chem Eur J*. 2018;24:14295-14301.
89. Cruz TR, Silva RA, Machado AE, et al. New DMSO–ruthenium catalysts bearing N-heterocyclic carbene ligands for the ring-opening metathesis of norbornene. *New J Chem*. 2019;43:6220-6227.
90. Samkian AE, Xu Y, Virgil SC, Yoon KY, Grubbs RH. Synthesis and activity of six-membered cyclic alkyl amino carbene–ruthenium olefin metathesis catalysts. *Organometallics*. 2020;39:495-499.
91. Aghahosseini H, Ramazani A, Gouranlou F, Joo SW. Nanoreactors technology in green organic synthesis. *Curr Org Synth*. 2017;14:810-864.
92. del Río E, Lligadas G, Ronda JC, et al. Shape memory polyurethanes from renewable polyols obtained by ATMET polymerization of glyceryl triundec-10-enoate and 10-undecenol. *Macromol Chem Phys*. 2011;212:1392-1399.
93. Rio ED, Lligadas G, Ronda J, et al. Polyurethanes from polyols obtained by ADMET polymerization of a castor oil-based diene: characterization and shape memory properties. *J Polym Sci A Polym Chem*. 2011;49:518-525.
94. Binder V, Bergum B, Jaisson S, et al. Impact of fibrinogen carbamylation on fibrin clot formation and stability. *Thromb Haemost*. 2017;117:899-910.
95. Walsh G. Post-translational modifications of protein biopharmaceuticals. *Drug Discov Today*. 2010;15:773-780.
96. Song K, Ye W, Gao X, et al. Synergy between dynamic covalent boronic ester and boron–nitrogen coordination: strategy for self-healing polyurethane elastomers at room temperature with unprecedented mechanical properties. *Mater Horiz*. 2021;8:216-223.
97. Peters JA. Interactions between boric acid derivatives and saccharides in aqueous media: structures and stabilities of resulting esters. *Coord Chem Rev*. 2014;268:1-22.
98. Suzuki A. Cross-coupling reactions of organoboranes: an easy way to construct C—C bonds (Nobel lecture). *Angew Chem Int Ed*. 2011;50:6722-6737.
99. Brown HC. Organoborane-carbon monoxide reactions. Synthesis of carbon structures. *Acc Chem Res*. 1969;2:65-72.
100. Lacina K, Skládal P. Ferroceneboronic acid for the electrochemical probing of interactions involving sugars. *Electrochim Acta*. 2011;56:10246-10252.
101. Xue CB, He X, Corbett RL, et al. Discovery of macrocyclic hydroxamic acids containing biphenylmethyl derivatives at p1', a series of selective TNF-α converting enzyme inhibitors with potent cellular activity in the inhibition of TNF-α release. *J Med Chem*. 2001;44:3351-3354.
102. Brooks WL, Sumerlin BS. Synthesis and applications of boronic acid-containing polymers: from materials to medicine. *Chem Rev*. 2016;116:1375-1397.
103. Piest M, Zhang X, Trinidad J, Engbersen JFJ. pH-responsive, dynamically restructuring hydrogels formed by reversible crosslinking of PVA with phenylboronic acid functionalised PPO–PEO–PPO spacers (Jeffamines®). *Soft Matter*. 2011;7:11111-11118.
104. Molander GA, Trice SL, Dreher SD. Palladium-catalyzed, direct boronic acid synthesis from aryl chlorides: a simplified route to

diverse boronate ester derivatives. *J Am Chem Soc*. 2010;132:17701-17703.
105. Roy D, Cambre JN, Sumerlin BS. Triply-responsive boronic acid block copolymers: solution self-assembly induced by changes in temperature, pH, or sugar concentration. *Chem Commun*. 2009;16:2106-2108.
106. Silva MP, Saraiva L, Pinto M, Sousa ME. Boronic acids and their derivatives in medicinal chemistry: synthesis and biological applications. *Molecules*. 2020;25:4323.
107. Di Giovannantonio M, Keerthi A, Urgel JI, et al. On-surface dehydro-Diels–Alder reaction of dibromo-bis (phenylethynyl) benzene. *J Am Chem Soc*. 2020;142:1721-1725.
108. Feng Z, Zuo H, Hu J, et al. In situ exfoliation of graphite into graphene nanosheets in elastomer composites based on Diels–Alder reaction during melt blending. *Ind Eng Chem Res*. 2019;58:13182-13189.
109. Tanasi P, Santana MH, Carretero-González J, et al. Thermoreversible crosslinked natural rubber: a Diels-Alder route for reuse and self-healing properties in elastomers. *Polymer*. 2019;175:15-24.
110. Nicolaou KC, Snyder SA, Montagnon T, Vassilikogiannakis G. The Diels–Alder reaction in total synthesis. *Angew Chem Int Ed*. 2002;41:1668-1698.
111. Brieger G, Bennett JN. The intramolecular Diels-Alder reaction. *Chem Rev*. 1980;80:63-97.
112. Boul PJ, Reutenauer P, Lehn JM. Reversible Diels—Alder reactions for the generation of dynamic combinatorial libraries. *Org Lett*. 2005;7:15-18.
113. Gheneim R, Perez-Berumen C, Gandini A. Diels—Alder reactions with novel polymeric dienes and dienophiles: synthesis of reversibly cross-linked elastomers. *Macromolecules*. 2002;35:7246-7253.
114. Zhao J, Xu R, Luo G, Wu J, Xia H. Self-healing poly(siloxane-urethane) elastomers with remoldability, shape memory and biocompatibility. *Polym Chem*. 2016;7:7278-7286.
115. Ninh C, Bettinger CJ. Reconfigurable biodegradable shape-memory elastomers via Diels–Alder coupling. *Biomacromolecules*. 2013;14:2162-2170.
116. Dondoni A. The emergence of thiol–ene coupling as a click process for materials and bioorganic chemistry. *Angew Chem Int Ed*. 2008;47:8995-8997.
117. Xue CH, Guo XJ, Zhang MM, Ma JZ, Jia ST. Fabrication of robust superhydrophobic surfaces by modification of chemically roughened fibers via thiol–ene click chemistry. *J Mater Chem A*. 2015;3:21797-21804.
118. Kade MJ, Burke DJ, Hawker CJ. The power of thiol-ene chemistry. *J Polym Sci A Polym Chem*. 2010;48:743-750.
119. Tucker-Schwartz AK, Farrell RA, Garrell RL. Thiol–ene click reaction as a general route to functional trialkoxysilanes for surface coating applications. *J Am Chem Soc*. 2011;133:11026-11029.
120. Cortez MA, Grayson SM. Thiol—ene click functionalization and subsequent polymerization of 2-oxazoline monomers. *Macromolecules*. 2010;43:4081-4090.
121. Jin Z, Xu B, Hammond GB. Green synthesis of vicinal dithioethers and alkenyl thioethers from the reaction of alkynes and thiols in water. *Eur J Org Chem*. 2010;2010:168-173.
122. Dai Y, Zhang X, Xia F. Click chemistry in functional aliphatic polycarbonates. *Macromol Rapid Commun*. 2017;38:1700357.
123. Wei H, Li Q, Ojelade M, Madbouly S, Otaigbe JU, Hoyle CE. Thiol—ene free-radical and vinyl ether cationic hybrid photopolymerization. *Macromolecules*. 2007;40:8788-8793.
124. Koo SP, Stamenović MM, Prasath RA, et al. Limitations of radical thiol-ene reactions for polymer–polymer conjugation. *J Polym Sci A: Polym Chem*. 2010;48:1699-1713.
125. Sinha AK, Equbal D. Thiol—ene reaction: synthetic aspects and mechanistic studies of an anti-Markovnikov-selective hydrothiolation of olefins. *Asian J Org Chem*. 2019;8:32-47.
126. Trofimova O, Grebneva E, Bolgova Y, et al. Anti-Markovnikov addition of 2-mercaptobenzoxazole and 2-mercaptobenzothiazole to trimethoxy (vinyl) silane under solvent-and catalyst-free conditions. *J Organomet Chem*. 2020;917:121269.
127. Fairbanks BD, Schwartz MP, Halevi AE, Nuttelman CR, Bowman CN, Anseth KS. A versatile synthetic extracellular matrix mimic via thiol-norbornene photopolymerization. *Adv Mater*. 2009;21:5005-5010.
128. Amato DV, Lee H, Werner G Jr, et al. Functional microcapsules via thiol–ene photopolymerization in droplet-based microfluidics. *ACS Appl Mater Interfaces*. 2017;9:3288-3293.
129. Black M, Rawlins JW. Thiol–ene UV-curable coatings using vegetable oil macromonomers. *Eur Polym J*. 2009;45:1433-1441.
130. Ma SJ, Mannino SJ, Wagner NJ, Kloxin CJ. Photodirected formation and control of wrinkles on a thiol–ene elastomer. *ACS Macro Lett*. 2013;2:474-477.
131. Hoyle CE, Bowman CN. Thiol–ene click chemistry. *Angew Chem Int Ed*. 2010;49:1540-1573.
132. Lowe AB. Thiol-ene "click" reactions and recent applications in polymer and materials synthesis. *Polym Chem*. 2010;1:17-36.
133. Nair DP, Podgórski M, Chatani S, et al. The thiol-Michael addition click reaction: a powerful and widely used tool in materials chemistry. *Chem Mater*. 2014;26:724-744.
134. Zhang B, Chakma P, Shulman MP, Ke J, Digby ZA, Konkolewicz D. Probing the mechanism of thermally driven thiol-Michael dynamic covalent chemistry. *Org Biomol Chem*. 2018;16:2725-2734.
135. Lewis CL, Meng Y, Anthamatten M. Well-defined shape-memory networks with high elastic energy capacity. *Macromolecules*. 2015;48:4918-4926.
136. Zeng D, Yang L, Fang T. Process optimization, kinetic and thermodynamic studies on biodiesel production by supercritical methanol transesterification with CH_3ONa catalyst. *Fuel*. 2017;203:739-748.
137. Zahir L, Kida T, Tanaka R, et al. Synthesis of thermoplastic elastomers with high biodegradability in seawater. *Polym Degrad Stab*. 2021;184:109467.
138. Bakkali-Hassani C, Poutrel Q-A, Langenbach J, et al. Lipase-catalyzed epoxy–acid addition and transesterification: from model molecule studies to network build-up. *Biomacromolecules*. 2021;22:4544-4551.
139. Feng Z, Hu J, Zuo H, et al. Photothermal-induced self-healable and reconfigurable shape memory bio-based elastomer with recyclable ability. *ACS Appl Mater Interfaces*. 2019;11:1469-1479.
140. Gao Y, Liu W, Zhu S. Reversible shape memory polymer from semicrystalline poly(ethylene-co-vinyl acetate) with dynamic covalent polymer networks. *Macromolecules*. 2018;51:8956-8963.
141. Rastogi P, Njuguna J, Kandasubramanian B. Exploration of elastomeric and polymeric liquid crystals with photothermal actuation: a review. *Eur Polym J*. 2019;121:109287.
142. Martella D, Parmeggiani C. Advances in cell scaffolds for tissue engineering: the value of liquid crystalline elastomers. *Chem Eur J*. 2018;24:12206-12220.
143. Saed MO, Volpe RH, Traugutt NA, Visvanathan R, Clark NA, Yakacki CM. High strain actuation liquid crystal elastomers via modulation of mesophase structure. *Soft Matter*. 2017;13:7537-7547.
144. Kularatne RS, Kim H, Boothby JM, Ware TH. Liquid crystal elastomer actuators: synthesis, alignment, and applications. *J Polym Sci B*. 2017;55:395-411.
145. Rousseau IA, Mather PT. Shape memory effect exhibited by smectic-C liquid crystalline elastomers. *J Am Chem Soc*. 2003;125:15300-15301.
146. Ahir SV, Tajbakhsh AR, Terentjev EM. Self-assembled shape-memory fibers of triblock liquid-crystal polymers. *Adv Funct Mater*. 2006;16:556-560.
147. Mehravar E, Iturrospe A, Arbe A, Asua JM, Leiza JR. Phase behavior of side-chain liquid-crystalline polymers containing biphenyl

mesogens with different spacer lengths synthesized via miniemulsion polymerization. *Polym Chem*. 2016;7:4736-4750.
148. Wolf JR. Review: main chain hydrogen-bonded liquid crystalline polymers. *Liquid Cryst Rev*. 2014;2:28-46.
149. Traugutt N, Volpe R, Bollinger M, et al. Liquid-crystal order during synthesis affects main-chain liquid-crystal elastomer behavior. *Soft Matter*. 2017;13:7013-7025.
150. Selinger JV, Jeon HG, Ratna B. Isotropic-nematic transition in liquid-crystalline elastomers. *Phys Rev Lett*. 2002;89:225701.
151. Fleischmann EK, Zentel R. Liquid-crystalline ordering as a concept in materials science: from semiconductors to stimuli-responsive devices. *Angew Chem Int Ed*. 2013;52:8810-8827.
152. Zubarev ER, Talroze RV, Yuranova TI, Plate NA, Finkelmann H. Influence of network topology on polydomain−monodomain transition in side chain liquid crystalline elastomers with cyanobiphenyl mesogens. *Macromolecules*. 1998;31:3566-3570.
153. Li Y, Pruitt C, Rios O, et al. Controlled shape memory behavior of a smectic main-chain liquid crystalline elastomer. *Macromolecules*. 2015;48:2864-2874.
154. Qin H, Mather PT. Combined one-way and two-way shape memory in a glass-forming nematic network. *Macromolecules*. 2009;42:273-280.
155. Guin T, Kowalski BA, Rao R, et al. Electrical control of shape in voxelated liquid crystalline polymer nanocomposites. *ACS Appl Mater Interfaces*. 2018;10:1187-1194.
156. Marotta A, Lama GC, Ambrogi V, Cerruti P, Giamberini M, Gentile G. Shape memory behavior of liquid-crystalline elastomer/graphene oxide nanocomposites. *Compos Sci Technol*. 2018;159:251-258.
157. Lama GC, Cerruti P, Lavorgna M, Carfagna C, Ambrogi V, Gentile G. Controlled actuation of a carbon nanotube/epoxy shape-memory liquid crystalline elastomer. *J Phys Chem C*. 2016;120:24417-24426.
158. Jin B, Song H, Jiang R, Song J, Zhao Q, Xie T. Programming a crystalline shape memory polymer network with thermo- and photo-reversible bonds toward a single-component soft robot. *Sci Adv*. 2018;4:eaao3865.
159. Torbati AH, Mather PT. A hydrogel-forming liquid crystalline elastomer exhibiting soft shape memory. *J Polym Sci B*. 2016;54:38-52.
160. Ube T, Kawasaki K, Ikeda T. Photomobile liquid-crystalline elastomers with rearrangeable networks. *Adv Mater*. 2016;28:8212-8217.
161. Liu W, Guo LX, Lin BP, Zhang XQ, Sun Y, Yang H. Near-infrared responsive liquid crystalline elastomers containing photothermal conjugated polymers. *Macromolecules*. 2016;49:4023-4030.
162. Umerova S, Kuscer D, Bobnar M, Derets N, Zalar B, Rešetič A. Shear flow-controlled shape memory of polymer resin dispersed liquid crystal elastomer microparticles. *Mater Des*. 2021;207:109836.
163. Wang Z, Tian H, He Q, Cai S. Reprogrammable, reprocessible, and self-healable liquid crystal elastomer with exchangeable disulfide bonds. *ACS Appl Mater Interfaces*. 2017;9:33119-33128.
164. Li Y, Rios O, Keum JK, Chen J, Kessler MR. Photoresponsive liquid crystalline epoxy networks with shape memory behavior and dynamic ester bonds. *ACS Appl Mater Interfaces*. 2016;8:15750-15757.
165. Zhai Y, Lados DA, LaGoy JL. Additive manufacturing: making imagination the major limitation. *JOM*. 2014;66:808-816.
166. Werner H, Dos Santos J, Fontes R, et al. Additive manufacturing models of fetuses built from three-dimensional ultrasound, magnetic resonance imaging and computed tomography scan data. *Ultrasound Obstet Gynecol*. 2010;36:355-361.
167. Ngo TD, Kashani A, Imbalzano G, Nguyen KTQ, Hui D. Additive manufacturing (3D printing): a review of materials, methods, applications and challenges. *Compos Part B Eng*. 2018;143:172-196.
168. Czyżewski J, Burzyński P, Gaweł K, Meisner J. Rapid prototyping of electrically conductive components using 3D printing technology. *J Mater Process Technol*. 2009;209:5281-5285.
169. Tofail SAM, Koumoulos EP, Bandyopadhyay A, Bose S, O'Donoghue L, Charitidis C. Additive manufacturing: scientific and technological challenges, market uptake and opportunities. *Mater Today*. 2018;21:22-37.
170. Vorndran E, Moseke C, Gbureck U. 3D printing of ceramic implants. *MRS Bull*. 2015;40:127-136.
171. Buchanan C, Gardner L. Metal 3D printing in construction: a review of methods, research, applications, opportunities and challenges. *Eng Struct*. 2019;180:332-348.
172. Stansbury JW, Idacavage MJ. 3D printing with polymers: challenges among expanding options and opportunities. *Dent Mater*. 2016;32:54-64.
173. Gosselin C, Duballet R, Roux P, Gaudillière N, Dirrenberger J, Morel P. Large-scale 3D printing of ultra-high performance concrete—a new processing route for architects and builders. *Mater Des*. 2016;100:102-109.
174. Derakhshanfar S, Mbeleck R, Xu K, Zhang X, Zhong W, Xing M. 3D bioprinting for biomedical devices and tissue engineering: a review of recent trends and advances. *Bioact Mater*. 2018;3:144-156.
175. Jiang Z, Diggle B, Tan ML, Viktorova J, Bennett CW, Connal LA. Extrusion 3D printing of polymeric materials with advanced properties. *Adv Sci*. 2020;7:2001379.
176. Wong KV, Hernandez A. A review of additive manufacturing. *Int Sch Res Notices*. 2012;2012:1-10.
177. Wang YJ, Jeng US, Hsu SH. Biodegradable water-based polyurethane shape memory elastomers for bone tissue engineering. *ACS Biomater Sci Eng*. 2018;4:1397-1406.
178. Xu C, Quinn B, Lebel LL, Therriault D, L'Espérance G. Multi-material direct ink writing (DIW) for complex 3D metallic structures with removable supports. *ACS Appl Mater Interfaces*. 2019;11:8499-8506.
179. Gibbs DM, Vaezi M, Yang S, et al. Hope versus hype: what can additive manufacturing realistically offer trauma and orthopedic surgery? *Regen Med*. 2014;9:535-549.
180. Jang T-S, Jung H-D, Pan MH, et al. *3D Printing of Hydrogel Composite Systems: Recent Advances in Technology for Tissue Engineering*. International Journal of Bioprinting; 2018.
181. Kuang X, Chen K, Dunn CK, Wu J, Li VCF, Qi HJ. 3D printing of highly stretchable, shape-memory, and self-healing elastomer toward novel 4D printing. *ACS Appl Mater Interfaces*. 2018;10:7381-7388.
182. Yu R, Yang X, Zhang Y, et al. Three-dimensional printing of shape memory composites with epoxy-acrylate hybrid photopolymer. *ACS Appl Mater Interfaces*. 2017;9:1820-1829.
183. Davidson EC, Kotikian A, Li S, Aizenberg J, Lewis JA. 3D printable and reconfigurable liquid crystal elastomers with light-induced shape memory via dynamic bond exchange. *Adv Mater*. 2020;32:1905682.
184. Kotikian A, Truby RL, Boley JW, White TJ, Lewis JA. 3D printing of liquid crystal elastomeric actuators with spatially programed Nematic order. *Adv Mater*. 2018;30:1706164.
185. Villacres J, Nobes D, Ayranci C. Additive manufacturing of shape memory polymers: effects of print orientation and infill percentage on shape memory recovery properties. *Rapid Prototyp J*. 2020;26:1593-1602.
186. Momeni F, Liu X, Ni J. A review of 4D printing. *Mater Des*. 2017;122:42-79.
187. Choi J, Kwon OC, Jo W, Lee HJ, Moon MW. 4D printing technology: a review. *3D Print Addit Manuf*. 2015;2:159-167.
188. Subash A, Kandasubramanian B. 4D printing of shape memory polymers. *Eur Polym J*. 2020;134:109771.
189. Liu Y, Zhang W, Zhang F, et al. Microstructural design for enhanced shape memory behavior of 4D printed composites based on carbon nanotube/polylactic acid filament. *Compos Sci Technol*. 2019;181:107692.

190. Tibbits S. 4D printing: multi-material shape change. *Archit Des*. 2014;84:116-121.
191. Baştanlar Y, Ozuysal M. Introduction to machine learning. *Methods Mol Biol*. 2014;1107:105-128.
192. Kauwe SK, Graser J, Murdock R, Sparks TD. Can machine learning find extraordinary materials? *Comput Mater Sci*. 2020;174:109498.
193. Zhang H, Moon SK. Reviews on machine learning approaches for process optimization in noncontact direct ink writing. *ACS Appl Mater Interfaces*. 2021;13:53323–53345.
194. Yan C, Feng X, Wick C, et al. Machine learning assisted discovery of new thermoset shape memory polymers based on a small training dataset. *Polymer*. 2021;214:123351.
195. Lin T-S, Coley CW, Mochigase H, et al. BigSMILES: a structurally-based line notation for describing macromolecules. *ACS Cent Sci*. 2019;5:1523-1531.
196. Dutta R, Renshaw D, Chen C, Liang D. Machine learning based approach for shape memory polymer behavioural characterization. *Array*. 2020;7:100036.
197. Hamel CM, Roach DJ, Long KN, Demoly F, Dunn ML, Qi HJ. Machine-learning based design of active composite structures for 4D printing. *Smart Mater Struct*. 2019;28:065005.
198. Scalet G. Two-way and multiple-way shape memory polymers for soft robotics: an overview. *Actuators*. Multidisciplinary Digital Publishing Institute; 2020:10.
199. Biswas MC, Chakraborty S, Bhattacharjee A, Mohammed Z. 4D printing of shape memory materials for textiles: mechanism, mathematical modeling, and challenges. *Adv Funct Mater*. 2021;31:2100257.
200. He Q, Wang Z, Song Z, Cai S. Bioinspired design of vascular artificial muscle. *Adv Mater Technol*. 2019;4:1800244.
201. Xiao M, Zhang N, Zhuang J, et al. Degradable poly (ether-ester-urethane) s based on well-defined aliphatic diurethane diisocyanate with excellent shape recovery properties at body temperature for biomedical application. *Polymers*. 2019;11:1002.
202. Worch JC, Weems AC, Yu J, et al. Elastomeric polyamide biomaterials with stereochemically tuneable mechanical properties and shape memory. *Nat Commun*. 2020;11:1-11.
203. Wang Y, Zhang P, Zhao Y, et al. Shape memory composites composed of polyurethane/ZnO nanoparticles as potential smart biomaterials. *Polym Compos*. 2020;41:2094-2107.
204. Ragin Ramdas M, Vijayalakshmi KP, Munirathnamma LM, Ravikumar HB, Santhosh Kumar KS. Shape memory polytriazole elastomers from aromatic monomers: synthesis and properties. *Mater Today Commun*. 2018;17:180-186.
205. Agrawal A, Yun T, Pesek SL, Chapman WG, Verduzco R. Shape-responsive liquid crystal elastomer bilayers. *Soft Matter*. 2014;10:1411-1415.
206. Roach DJ, Yuan C, Kuang X, et al. Long liquid crystal elastomer fibers with large reversible actuation strains for smart textiles and artificial muscles. *ACS Appl Mater Interfaces*. 2019;11:19514-19521.
207. Gavin TP. Clothing and thermoregulation during exercise. *Sports Med*. 2003;33:941-947.
208. Ji F, Li JB, Weng YX, Ren J. Synthesis of PLA-based thermoplastic elastomer and study on preparation and properties of PLA-based shape memory polymers. *Mater Res Express*. 2020;7:14.
209. Haines CS, Lima MD, Li N, et al. Artificial muscles from fishing line and sewing thread. *Science*. 2014;343:868-872.
210. Kim J, Kim JW, Kim HC, Zhai L, Ko HU, Muthoka RM. Review of soft actuator materials. *Int J Precis Eng Manuf*. 2019;20:2221-2241.
211. Ekbatani RZ, Shao K, Khawwaf J, et al. Control of an IPMC soft actuator using adaptive full-order recursive terminal sliding mode. *Actuators*. 2021;10:33.
212. Panahi-Sarmad M, Abrisham M, Noroozi M, et al. Programing polyurethane with rational surface-modified graphene platelets for shape memory actuators and dielectric elastomer generators. *Eur Polym J*. 2020;133:109745.
213. Koerner H, Price G, Pearce NA, Alexander M, Vaia RA. Remotely actuated polymer nanocomposites—stress-recovery of carbon-nanotube-filled thermoplastic elastomers. *Nat Mater*. 2004;3:115-120.
214. Rossiter J, Takashima K, Mukai T. Shape memory properties of ionic polymer–metal composites. *Smart Mater Struct*. 2012;21:112002.
215. Shen Q, Trabia S, Stalbaum T, Palmre V, Kim K, Oh IK. A multiple-shape memory polymer-metal composite actuator capable of programmable control, creating complex 3D motion of bending, twisting, and oscillation. *Sci Rep*. 2016;6:24462.
216. Chen H, Xia H, Qiu Y, Xu Z, Ni QQ. Smart composites of piezoelectric particles and shape memory polymers for actuation and nanopositioning. *Compos Sci Technol*. 2018;163:123-132.
217. Chen H, Xia H, Ni Q-Q. Study on material performances of lead zirconate titanate/shape memory polyurethane composites combining shape memory and piezoelectric effect. *Compos A: Appl Sci Manuf*. 2018;110:183-189.
218. Bodkhe S, Ermanni P. 3D printing of multifunctional materials for sensing and actuation: merging piezoelectricity with shape memory. *Eur Polym J*. 2020;132:109738.
219. Kent TA, Ford MJ, Markvicka EJ, Majidi C. Soft actuators using liquid crystal elastomers with encapsulated liquid metal joule heaters. *Multifunct Mater*. 2020;3:025003.
220. Pringpromsuk S, Xia H, Ni Q. Multifunctional stimuli-responsive shape memory polyurethane gels for soft actuators. *Sens Actuators A-Phys*. 2020;313:112207.
221. Liu Y, Du H, Liu L, et al. Shape memory polymers and their composites in aerospace applications: a review. *Smart Mater Struct*. 2014;23:023001.
222. Arun DI, Santhosh Kumar KS, Satheesh Kumar B, Chakravarthy P, Dona M, Santhosh B. High glass-transition polyurethane-carbon black electro-active shape memory nanocomposite for aerospace systems. *Mater Sci Technol*. 2019;35:596-605.
223. Dao TD, Ha NS, Goo NS, Yu WR. Design, fabrication, and bending test of shape memory polymer composite hinges for space deployable structures. *J Intell Mater Syst Struct*. 2018;29:1560-1574.
224. Akbari S, Sakhaei AH, Kowsari K, et al. Enhanced multimaterial 4D printing with active hinges. *Smart Mater Struct*. 2018;27:065027.
225. Gong X, Tan K, Deng Q, Shen S. Athermal shape memory effect in magnetoactive elastomers. *ACS Appl Mater Interfaces*. 2020;12:16930-16936.
226. Zhang X, Cai J, Liu W, Liu W, Qiu X. Synthesis of strong and highly stretchable, electrically conductive hydrogel with multiple stimuli responsive shape memory behavior. *Polymer*. 2020;188:122147.
227. Tang Z, Huang J, Guo B, Zhang L, Liu F. Bioinspired engineering of sacrificial metal–ligand bonds into elastomers with supramechanical performance and adaptive recovery. *Macromolecules*. 2016;49:1781-1789.
228. Ube T, Tsunoda H, Kawasaki K, Ikeda T. Photoalignment in polysiloxane liquid-crystalline elastomers with rearrangeable networks. *Adv Opt Mater*. 2021;9:2100053.
229. Michal BT, McKenzie BM, Felder SE, et al. Metallo-, thermo-, and photoresponsive shape memory and actuating liquid crystalline elastomers. *Macromolecules*. 2015;48:3239-3246.
230. Lai SM, Wang XF. Shape memory properties of olefin block copolymer (OBC)/poly (ε-caprolactone) (PCL) blends. *J Appl Polym Sci*. 2017;134:45475.
231. Hsu Y-H, Luong D, Asheghali D, Dove AP, Becker ML. Shape memory behavior of biocompatible polyurethane stereoelastomers synthesized via thiol–Yne Michael addition. *Biomacromolecules*. 2022. https://pubs.acs.org/doi/abs/10.1021/acs.biomac.1c01473
232. Li Z, Li K, He H, Zhou Y, He Z. Tough and tunable shape memory PLA/PAE melt-blends actuated by temperature. *Iran Polym J*. 2019;28:371-378.

233. Yang W, Guan D, Liu J, Luo Y, Wang Y. Synthesis and characterization of biodegradable linear shape memory polyurethanes with high mechanical performance by incorporating novel long chain diisocyanates. *New J Chem*. 2020;44:3493-3503.
234. Liu B, Tang Z, Wang Z, Zhang L, Guo B. Integrating transient and sacrificial bonds into biobased elastomers toward mechanical property enhancement and macroscopically responsive property. *Polymer*. 2019;184:121914.
235. Wang C, Wang H, Zou F, Chen S, Wang Y. Development of polyhydroxyalkanoate-based polyurethane with water-thermal response shape-memory behavior as new 3D elastomers scaffolds. *Polymers*. 2019;11:1030.
236. Zhao W, Liu Y, Zhang Z, et al. High-strength, fast Self-healing, aging-insensitive elastomers with shape memory effect. *ACS Appl Mater Interfaces*. 2020;12:35445-35452.
237. Zhang X, Zhu C, Xu B, Qin L, Wei J, Yu Y. Rapid, localized, and athermal shape memory performance triggered by photoswitchable glass transition temperature. *ACS Appl Mater Interfaces*. 2019;11:46212-46218.
238. Ramaraju H, Ul-Haque A, Verga AS, Bocks ML, Hollister SJ. Modulating nonlinear elastic behavior of biodegradable shape memory elastomer and small intestinal submucosa (SIS) composites for soft tissue repair. *J Mech Behav Biomed Mater*. 2020;110:103965.
239. Lee D-H, Chang Y-W, Jang K-S. Morphology, mechanical properties and shape memory effects of Polyamide12/polyolefin elastomer blends Compatibilized by Glycidylisobutyl POSS. *Materials*. 2021;14:27.
240. Krajovic DM, Anthamatten M. Melt-processable shape-memory elastomers containing Bisurea segments. *ACS Appl Polym Mater*. 2021;3:2082-2087.
241. Das R, Banerjee SL, Kumar R, Kundu PP. Development of sustainable elastomeric engineering nanocomposites from linseed oil with improved mechanical stability and thermally induced shape memory properties. *J Ind Eng Chem*. 2016;35:388-399.
242. Chen Z, Li Y, Yao C. Biomass shape memory elastomers with rapid self-healing properties and high recyclability. *Biomacromolecules*. 2021;22:2768-2776.

How to cite this article: Prathumrat P, Nikzad M, Hajizadeh E, Arablouei R, Sbarski I. Shape memory elastomers: A review of synthesis, design, advanced manufacturing, and emerging applications. *Polym Adv Technol*. 2022;33(6):1782-1808. doi:10.1002/pat.5652